River quality monitoring with Image analysis

Domenico Miglino

Dipartimento di Ingegneria Civile, Edile e Ambientale

Università degli Studi di Napoli Federico II

Thesis submitted for the degree of PhD in Civil Systems Engineering

Napoli, November 2024

PhD Supervisors

Prof. Salvatore Manfreda, Università degli Studi di Napoli Federico II,

Prof. Francesco Isgrò, Università degli Studi di Napoli Federico II

PhD Thesis Reviewers

Dr. Seifeddine Jomaa, Helmholtz Centre for Environmental Research - UFZ

Dr. Patricia Lourenco, University of Evora Mediterranean Institute for Agriculture Environment and Development

PhD Programme Coordinator - XXXVII Cycle

Prof. Andrea Papola, Università degli Studi di Napoli Federico II

Abstract

Fresh water is becoming a more and more valuable resource which deserves to be properly managed and wisely preserved, exploiting all available techniques and knowledges.

In this context, water turbidity is an essential proxy for assessing river quality and protecting aquatic ecosystems, since it is linked to the presence of organic and inorganic suspended matter. Current monitoring practices are mainly limited by low spatial and temporal resolution, and high costs, preventing the achievement of extensive and timely water quality information at global scale. Digital cameras can overcome these constraints, providing significant advantages to existing techniques. This study proposes an image analysis procedure for river turbidity assessment under varying hydrological conditions. Several turbidity events were artificially re-created on site during the real-scale tests using clay tracers with different colors and concentrations, also varying camera types and installation setups, for the optimization of the monitoring system. The experimental validation of the data was performed by installing two turbidimeters within the river section. The field tests revealed that environmental and hydrological long-term factors, including the characteristics of suspended particles, water level, and light condition, influence the effectiveness of the method. Riverbed background reflectance should also be taken into account because it could strongly modify the total water upwelling light, especially for shallow waters. Considering all these variables, the results showed that for short-term experiments (minutes, hours) the camera single bands values, in particular red band, seems to be the most reliable indicator for estimating water turbidity, better than bands ratios. Instead, for long-term monitoring (days, seasons), the single bands reflectance tends to be more influenced by light and river flow variations, while bands ratios performances start to increase. The purpose of this work is to deepen the implementation of this camera system in real-world settings to support existing river monitoring practices with early warning networks and to aid in developing new solutions for water resources management.

Keywords: river monitoring, water quality, image processing, turbidity, camera systems.

Abstract (Ita)

L'acqua diventerà una risorsa sempre più preziosa da gestire adeguatamente e preservare saggiamente, sfruttando tutte le tecniche e conoscenze a disposizione.

In questo contesto, la torbidità dell'acqua è un indicatore essenziale per valutare la qualità dei fiumi e salvaguardare gli ecosistemi acquatici, poiché è legata alla presenza di materia organica e inorganica in sospensione. Le attuali pratiche di monitoraggio sono principalmente limitate da una bassa risoluzione spaziale e temporale, oltre che da alti costi, impedendo di ottenere informazioni diffuse e tempestive sulla qualità dell'acqua a scala globale. Le fotocamere digitali possono superare queste limitazioni, offrendo vantaggi significativi alle tecniche esistenti. Questo studio propone una procedura di analisi delle immagini per la valutazione della torbidità dei fiumi in condizioni idrologiche variabili. Diversi eventi di torbidità sono stati ricreati artificialmente in sito durante i test a scala reale utilizzando traccianti di argilla con colori e concentrazioni differenti, variando anche i tipi di fotocamere e le configurazioni di installazione, per ottimizzare il sistema di monitoraggio. La validazione sperimentale dei dati è stata effettuata installando due turbidimetri nella sezione del fiume. I test sul campo hanno rivelato che fattori ambientali e idrologici a lungo termine, inclusi le caratteristiche delle particelle sospese, il livello dell'acqua e le condizioni di luce, influenzano l'efficacia del metodo. Anche la riflettanza del fondo del letto del fiume deve essere tenuta in conto poiché potrebbe modificare notevolmente la luce totale riflessa dall'acqua, specialmente in acque poco profonde. Considerando tutte queste variabili, i risultati hanno mostrato che per esperimenti a breve termine (minuti, ore) i valori delle singole bande della fotocamera, in particolare la banda del rosso, sembrano essere l'indicatore più affidabile per stimare la torbidità dell'acqua, piuttosto che gli indici che includono più bande. Invece, per il monitoraggio a lungo termine (giorni, stagioni), la riflettanza delle singole bande tende a essere più influenzata dalle variazioni di luce e delle condizioni idrauliche, mentre le prestazioni degli indici iniziano a migliorare. Lo scopo di questo lavoro è approfondire l'implementazione di questo sistema di fotocamere in contesti reali per supportare le pratiche esistenti di monitoraggio dei fiumi con reti di preallerta ed aiutare nello sviluppo di nuove soluzioni per la gestione delle risorse idriche.

Keywords: monitoraggio dei fiumi, qualità dell'acqua, elaborazione delle immagini, torbidità, fotocamere.

Graphical abstract

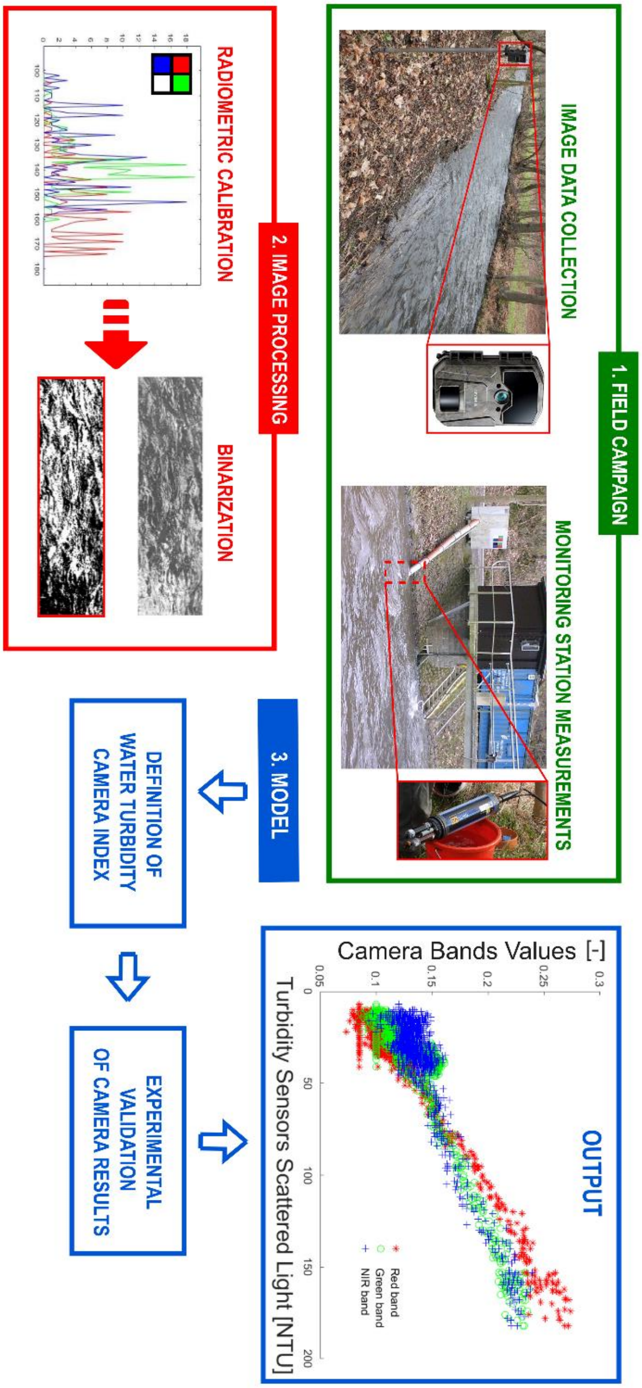

Acknowledgements

PhD isn't an easy path to take and complete, if you are not guided by the right people and purposes.

I would thank Prof. Salvatore Manfreda for showing me his enthusiastic and holistic approach to research and the positive mindset to face the issues, because "se non sbagli, non impari".

I would also mention the great help for my field work received by Dr. Seifeddine Jomaa, Prof. Michael Rode, Uwe Kiwel and my friend Mohammed.

I would thank my father, Pino, for supporting me in his own way, yelling at me with no reason every day of my life.

I would like to thank my dog, Arya, for having once bitten his hand.

I would like to thank my mother, for making me understand the importance of kindness and the real valuable things.

I would like to thank all my cousins, aunts, uncles and grandparents, for never making me feel alone.

I would like to thank Federica for cheering my days with her smiles and funny complaints.

I would like to thank my Agropoli's "conoscenti" for all the rich moments spent together during these years, making me forget how poor can be a researcher.

I would like to thank my Napoli's friends and "copilots" for all the beers, the football matches and their generosity for letting me win a lot of fantacalci, let's say easily.

I would like all my friends and colleagues of the DICEA family, for making this work experience unforgettable with all the coffee breaks, parties, dinners and travels together.

Finally, I would like to thank myself… No, just kidding.

Sincerely,

Mimmo

Napoli, November 2024

I jumped in the river and what did I see?

All my past and futures.

There was nothing to fear and nothing to doubt.

[Radiohead]

Table of Contents

List of Figures

List of Tables

Abbreviations: Acronyms and scientific units

BG - Background

CW - Clear water

LRB - Left riverbank

MSC - Multispectral camera

NTU - Nephelometric turbidity unit

RCP - Radiometric calibration panel

RGB – Red, green and blue: colour representation model used on the digital screen

ROI - Region of interest

RRB - Right riverbank

TC - Trap camera

UAS - Unmanned Aerial System

UAV - Unmanned Aerial Vehicle

DN - Digital number [-]

PI - Pixel intensity [-]

IR - Solar irradiance [W/m^2]

NDTI - Normalize difference turbidity index [-]

NDWI - Normalize difference water index [-]

NIR - Near-infrared radiation band [0.78–3 μm]

R_b - Reflectance of the riverbed background [-]

R_0 - Single band value for clear water condition [-]

RV_{rc} - RGB bands reference value of the radiometric calibration panel [-]

R_s - Reflectance of the suspended particles [-]

R_w - Reflectance of the water [-]

SSC - Suspended sediment concentration [gr/l]

1 Introduction

Water resources management is facing critical challenges due to the combined effects of global warming, population growth, human pressures, and increased pollution. These factors collectively contribute to the global rise in hydrological extremes, including droughts and floods. Furthermore, they exacerbate the declining trend in water availability and the degradation of water quality, which could ultimately result in chronic water scarcity affecting a substantial portion of the world's population.

The very recent Water Framework Directive report on Europe's water quality of October 2024 (https://www.eea.europa.eu/en/analysis/publications/europes-state-of-water-2024) references data from 2021, showing that only 37% of surface waters achieved good ecological status, and 29% met good chemical standards. Groundwater performed better, with 77% in good chemical condition, but remain concerns about pollution and pressures from agriculture.

In addition, water quality is being degraded more rapidly and diversely than ever, with an increasing number of pollutants such as nutrients, pesticides, plastics, and emerging contaminants (Bhateria & Jain,2016; Hannah et al., 2022).

To address these challenges effectively, the field of water resources monitoring must evolve by considering the complex interconnections between the environment and human society (Montanari et al., 2013; Ross & Chang, 2020).

Although the existing and commonly used monitoring systems have laid the foundation for our knowledge, these were designed under different hydrological conditions compared to today's needs and challenges. These monitoring systems are laborious and expensive, and often provide data that is discontinuous in space and time (Sergeant & Nagorski, 2015). For example, current low-frequency water quality sampling methods fail to capture occasional pollution events or changes induced by urban floods, while high-frequency monitoring approaches using in situ water quality sensors are more likely to detect these dynamics in a detailed manner (e.g. Outram et al., 2014). However, these approaches are prone to instrument degradation (e.g. biofouling, calibration issues) and human error, if adequate instrumental maintenance and technical staff training are not ensured. Thus, it is necessary to adopt new observational strategies, benefiting from the increasing technological development, to deepen comprehension and gain further insights on river ecosystems and dynamics.

Advancements are expected to enhance the spatiotemporal resolution of observations in order to improve “near real-time” water quality and quantity monitoring to move towards more equitable, sustainable and efficient water management. In fact, water management practices face limitations concerning data availability and timely data sharing, especially in rapidly changing environments. Increasing in-depth knowledge of how climate change as well as human pressures impact the environment, in both time and space, cannot be achieved solely with traditionally used instruments. Furthermore, the absence of a data-sharing policy in certain regions, coupled with the lack of common standards and protocols for hydrological monitoring, metadata storage, and exchanges – especially for qualitative monitoring – presents additional challenges to achieving effective and sustainable water management.

Recent advancements in new sensor technologies, and unmanned aerial systems (UASs), present promising opportunities to revolutionize environmental monitoring (Demarchi et al., 2017, Koparan et al., 2018, 2020; Manfreda et al., 2018, Wang & Yang, 2019; Perks et al., 2020; Piégay et al., 2020; Taramelli et al., 2020; Strelnikova et al., 2023). Furthermore, the integration of groundbased measurements with remotely acquired data makes it possible to characterize environmental processes much more accurately than in the recent past.

A new approach to hydrological monitoring can start by exploiting the capabilities of remote sensing, camera systems mounted on UASs or in fixed locations and image processing algorithms. These methods and approaches may provide complementary and valuable information as well as processing capabilities to comprehensively monitor fluvial systems.

1.1 Hydrological monitoring constraints

Effective hydrological monitoring faces several challenges to ensure sustainable and equitable water resources management. This section will discuss three key challenges: data scarcity and institutional limitations, spatial and temporal variability, and increasing demands for water resources.

1.1.1 Data scarcity and institutional limitations

The primary challenge in hydrological monitoring is data scarcity. Traditional monitoring systems often suffer from inadequate spatial coverage, limited temporal resolution, and insufficient availability of data. This scarcity of data hinders the accurate assessment of water resources and their quality, making it difficult to develop robust management strategies.

One of the most pressing concerns in data collection is the fragmentation of agencies and institutions responsible for overseeing distinct monitoring networks aimed at various objectives while tracking the same variables. This results in a heterogeneous and non-uniform distribution of monitoring stations, which often lack connections to a shared database or are installed at locations not suitable for specific objectives (Kirchner, 2006). Despite the overall increase in the number of sensors deployed over time, the availability of pertinent information has not shown significant improvement. The development of monitoring systems over time has been significantly shaped by political decisions and monosectorial water management criteria that lead to fragmented networks.

Water quality monitoring is probably one of the most complex activities which frequently implies field sampling standards, complex laboratory protocols and techniques as well as routine data analysis. The Waterbase European Environment Agency (EEA) databases report on the status and quality of Europe's rivers, lakes, groundwater bodies and transitional, coastal, and marine waters, on the quantity of Europe's water resources, and on the emissions to surface waters from point and diffuse sources of pollution (Waterbase – Water Quality ICM, 2022). This data shows that there are about 1550 monitoring locations, distributed over 24 European countries, having three or more years of data with an average of at least four samples per year. This database represents just a subset of the EU Water Quality Monitoring Network, but the limited temporal resolution of most of the water quality observations does not allow researchers to capture the variability of natural and anthropic processes especially with respect to pollution events (Alilou et al., 2019). At a global scale, the Global Database of Freshwater Quality (GEMStat, https://gemstat.org/) is one of the most comprehensive repositories of measured water quality data and gathered with voluntary submissions from different countries and organizations. The GEMStat database contains over 15 million entries from about 130,000 stations gathered from more than 80 countries (https://gemstat.org/about/dataavailability/). Even if many gauging stations contain only a small fraction of available data, the GEMStat database represents an important open-access and valuable reference for in situ water quality at global scale.

To address this limitation, the GlobeWQ project (https://www.globewq.info/) advanced global water quality assessments, using a combination of data from in situ monitoring, modeling and remote sensing, the so called "triangulation approach", detecting for example critical pollution hotspots in Africa and Asia. Its predictive models highlight the worsening of water quality trends by 2050 without stronger interventions. Regional case studies, such as Lake Victoria, showcase the platform's capacity for targeted water quality management

1.1.2 Spatial and temporal variability

Another significant challenge is represented by the spatial and temporal variability of hydrological processes and water resources. Their patterns exhibit substantial variations and are influenced by factors such as climate, land use, soil characteristics, morphology, human activities, and interventions. Traditional monitoring systems, often based on pointwise measurements or sampling, struggle to adequately capture this variability. In fact, the hydrological variables are mutually influenced and controlled by the spatial variability of physical factors (e.g. Rodríguez-Iturbe et al., 2006; Metzger et al., 2017; Meijer et al., 2021). Therefore, water resource regimes can differ significantly between and within river basins due to the heterogeneity of geological settings, land cover, soil types, and human pressures. To account for this variability, monitoring networks must be designed to capture such heterogeneities. This requires the optimal distribution and densification of monitoring stations, and the use and integration of remote sensing data to gather spatially explicit information. This is also a clear objective introduced by the Water Framework Directive 2000/60/EC (WFD), although it is not always fully implemented, due to tangible limitations (e.g. insufficient funding, lack of skilled human resources).

Temporal variability also poses an additional challenge for water availability and quality monitoring. Infrequent sampling and sparse data collection fail to adequately capture water dynamics that can vary dramatically over different time scales, ranging from hourly fluctuations to seasonal variations, and long-term trends. Therefore, high-frequency monitoring, enabled by advanced sensor technologies and automated data collection systems, is crucial for accurately capturing these processes (e.g. Rode et al., 2016).

1.1.3 Increasing demands for water resources

Population growth, urbanization, and industrial development exert pressure on water availability and quality. This pressure is emphasized by the current and likely future impacts of climate change on water resources. Balancing the competing demands for water resources while ensuring their sustainable use and allocation requires monitoring networks which can be expanded and upgraded to provide comprehensive coverage and real-time data. However, traditional monitoring approaches often struggle to keep pace with the increasing demands for data.

Furthermore, as water scarcity becomes more and more pressing, efficient water management strategies are needed to optimize water allocation and minimize waste. Integrated monitoring systems that combine hydrological data with socio-economic information can facilitate informed decision making and support sustainable water resources management. Addressing the challenges of data scarcity and limitations, spatial and temporal variability, and increasing demands for water resources requires a concerted effort from the scientific community, policy- and decision makers, and water resources managers. These challenges are clearly identified by the IAHS Water Solutions Decade on "Science for Solutions: Hydrology Engaging Local People IN one Global world (HELPING)." In this context, Theme 3 is promoting joint efforts to integrate new technologies with existing ones (IAHS, 2023).

1.2 New opportunities in hydrological monitoring

Fast-developing technologies such as remote sensing, UAS, advanced sensor networks, and wireless data networks offer opportunities to improve data availability and accessibility, and to collect data more efficiently and comprehensively. These technologies can also provide relatively high-resolution data over large spatial extents and properly capture temporal variations of hydrological processes. Integration of these technologies with data-driven approaches, such as AI, can enable more accurate and reliable hydrological monitoring.

This section will explore key areas such as: remote sensing, sensor networks and citizen science.

1.2.1 Remote sensing

Satellite-based technologies offer the main advantage of wide-area coverage, capturing information on various hydrological variables such as precipitation, evapotranspiration, soil moisture, and surface water dynamics (Chen & Wang,2018, Pereira et al., 2019, Albertini et al., 2022). This data, depending on the satellite mission characteristics, can be obtained at reasonable regular time intervals and at varying costs (some data are also available for free, such as those from the Copernicus mission), allowing for the assessment of temporal changes and the characterization of spatial patterns.

Numerous observation systems are tailored for hydrological research. Within National Aeronautics and Space Administration (NASA's) 19 Earth science missions, nine are notably pertinent to hydrology: AQUA, ICESat-2, GPM, GRACE, PMM, SLAP, SMAP, SWOT, and VIIRS (NASA,2023). ESA has four missions relevant to hydrology: CryoSat-2, EUMETSAT satellites, Copernicus Sentinel-1 and Sentinel-2, and SMOS (Soil Moisture and Ocean Salinity) (ESA,2023). ESA intends to launch the EarthCARE mission to enhance understanding of clouds and aerosols' role in solar radiation reflection. China has made substantial progress in Earth hydrology-related observation with the Fengyun and Haiyang satellite series, which focuses on meteorological observations and oceanographic monitoring, and plans to also launch the Water Cycle Observation Mission (WCOM) (Shi et al., 2016).

In addition, various national and international initiatives aim to advance the intersection of EO and hydrological science. These include the International Precipitation Working Group (IPWG), NASA Energy and Water Cycle Study (NEWS), European Union WATer and Global CHange (WATCH), and the Global Energy and Water Exchanges (GEWEX,2018) initiative.

The combined efforts of EO missions and initiatives are propelling hydrology into the era of "big data" (Peters-Lidard et al., 2017). Big data techniques can handle vast amounts of data, extract meaningful insights and interpret complex hydrological datasets, leading to improved understanding and predictive capabilities.

UASs, alongside satellites, are also valuable tools for hydrological monitoring (Manfreda & Ben Dor, 2023). These systems use advanced sensors to collect high-resolution data on a local scale, allowing for precise observations. UASs are versatile and agile, capable of capturing RGB and multi- or hyper-spectral data, thermal imagery, and light detection and ranging (LiDAR) data. They excel in covering local to large areas, reaching inaccessible regions and improving the spatial and temporal resolution of hydrological observations. Currently, one limitation for the use of UASs is the maximum extent of individual surveys. Swarm drone operations could overcome these limitations using multiple unmanned aerial platforms carrying sensors integrated as a single networked system.

In this context, an intermediate level between satellites and UASs is represented by "CubeSat" and High-Altitude Pseudo Satellites (HAPS), which offer the possibility of conducting surveys over larger surfaces with high resolution. CubeSats are nano satellites which have standardized size and form which are increasingly utilized by space agencies (McCabe et al., 2017). HAPS, which typically fly at 15 000–30 000 m above ground level for several months at a time, are also currently in development and testing. Both systems have the potential to fill the gap between satellites and UAS for EO and hydrological monitoring, given their endurance and spatial resolution (Poghosyan & Golkar, 2017; Gonzalo et al., 2018; Baraniello et al., 2021).

1.2.2 Internet of Things (IoT) and sensor networks

The Internet of Things (IoT) represents a novel technological paradigm conceptualized as a worldwide network of machines and devices with the ability to engage in mutual interactions (Lee & Lee,2015). It allows the integration of sensors interconnected through a variety of access networks, facilitated by cutting-edge technologies like embedded sensing and actuation, radio frequency identification (RFID), wireless networks, and semantic and real-time web services. The IoT's low-power wide-area network (LPWAN) capabilities enable the utilization of battery-powered sensors. Among these, long-range wide-area network (LoRaWAN) stands out as it employs open-source technology and operates on unlicensed frequency bands, offering significantly greater range compared to WiFi or Bluetooth connections. LoRaWAN is particularly advantageous for applications in remote regions where cellular networks experience limited coverage. Given the multitude of devices that can be connected, the number of local measurements could enormously increase, offering the possibility to further explore complex dynamics of hydrological forcings (Perumal et al., 2015; Balsamo et al., 2018; Tauro et al., 2018a; Tosi et al., 2020; Livoroi et al., 2021).

Sensory networks, in conjunction with IoT, hold promising potential for adaptive monitoring strategies through dynamic adjustments to the spatial distribution and density of sensors based on evolving hydrological conditions. Such flexibility enables targeted data collection in response to specific events or areas of interest, incorporating event-based triggers for sensor readings. Consequently, this approach optimizes the allocation of monitoring resources (Marino et al., 2023; Zanella et al., 2023).

1.2.3 Citizen science and crowd-sourced data

Citizen science represents an innovative tool with a measurable influence on environmental stewardship and public policy advocacy. When integrated with crowdsourcing, involving the gathering of extensive data from a diverse array of participants, citizen engagement can lead to an immediate, real-time response to pressing issues, such as pollution and natural disasters. Engaging the public in data collection and classification not only increases data coverage but also promotes public awareness and participation in water resources management (e.g. Sermet et al., 2020; Nardi et al., 2022).

Recently, several initiatives have stimulated the participation of volunteers in data collection through methods such as mobile applications, community-based monitoring programmes, or distributed sensor networks – as is the case, for example, with the CrowdWater project (Strobl et al., 2019). Participants can measure water levels and discharge, report on water quality observations, and share hydrological data collected from their personal monitoring stations. This collaborative effort significantly boosts data availability and offers valuable insights into the specific hydrological conditions within local areas, while also providing an avenue for active participation of key stakeholders in the community to foster technology localization and sustainability. The use of crowd-sourced data also holds the potential to complement conventional monitoring networks by capturing detailed spatial and temporal data (e.g. Etter et al., 2020; Mapiam et al., 2022).

In this context, citizen-acquired data may not always be comparable to professionally obtained data. To maintain high data quality standards, initiatives in citizen science consistently incorporate training and implement measures for quality control. This enables participants to contribute effectively, following simple and reliable procedures. Integration of these data with professional monitoring data, remote sensing observations, or model simulations can notably enhance the accuracy and resolution of hydrological analyses. Several private sensor networks have grown significantly in the last few years, producing many measurements that may be easily filtered and validated and offering a dense network of observations (de Vos et al., 2019). Popular online platforms such as Netatmo (https://weathermap.netatmo.com) and Weather Underground (https://www.wunderground.com/) collect and visualize measurements from public and even personal weather stations (PWSs) every ~5 to 10 min with a total number of sensors that exceeds by one order of magnitude the number of stations of the national hydrological services (Coney et al., 2022).

This private network of rainfall stations connected to a web service has been clearly assessed in a recent work by Graf et al. (2021). In fact, these opportunistic networks can lead, after filtering and sensor calibration (Krüger et al., 2023), to rainfall maps of higher accuracy and increased spatial variability, especially on smaller spatial and temporal scales.

The successful use of citizen science's potential for hydrological monitoring relies on a crucial collaboration between scientists, water managers, and the public. This engagement with the public also proves to be an effective approach for fostering a deeper understanding of water level measurements, discharge estimates, water conservation and shoreline changes (Harley et al., 2019; Seibert et al., 2019; Wang et al., 2022).

Several citizen science initiatives and crowd-sourced data collection platforms can contribute to data integration efforts (for instance, the largest people-powered research platform, Zooniverse – https://www.zooniverse.org/). Engaging the public in data collection and monitoring processes can increase data coverage and improve community involvement in water management decisions. This approach has been used, for instance, for flood risk management in Argentina, France, and New Zealand (e.g. Le Coz et al., 2016) and for coastal litter monitoring (e.g. van Lieshout et al., 2020).

1.3 Image analysis for river monitoring

The proliferation of modern optical sensors, present in satellites, on UASs, and in smartphones as well as attached to low-cost single-board computers or micro-controllers, has sparked a compelling interest in utilizing imagery to greatly broaden the scope of possible hydrological observations. Digital cameras have been successfully used in areas such as surveillance, facial recognition, object detection and tracking, inventory monitoring, and management. Additionally, some existing algorithms developed for general purposes have found intriguing applications in environmental monitoring, including the creation of three-dimensional (3D) models (James et al., 2019), assessment of highway vehicle flux (Hsu et al., 2003), monitoring air pollution (Zhang et al., 2016), measuring rainfall intensity (Allamano et al., 2015; Kavian et al., 2018; Jiang et al., 2019), and mapping river velocity fields (Johnson & Cowen, 2017; Lewis & Rhoads, 2018), among others.

Numerous researchers are currently delving into the field of river monitoring using image processing techniques. This includes a range of possibilities like traditional image processing methods from computer vision, but also new techniques utilizing AI.

It is becoming increasingly common for ordinary hydrological stations to be associated with nearby installed optical cameras. New camera systems have the potential to capture a range of complementary information, such as water level, velocity, and water quality parameters, useful for interpreting natural phenomena. They may also be exploited to measure features with the support of an evolving range of software and tools.

1.3.1 Remote sensing of water quality

Numerous water quality parameters serve as key pollution indicators. Gholizadeh et al. (2016) identifies a list of most commonly measured qualitative parameters of water, which include chlorophyll-a, Secchi disk depth, temperature, coloured dissolved organic matter, total organic carbon, dissolved organic carbon, total suspended matter, turbidity, sea surface salinity, total phosphorus, ortho-phosphate, chemical oxygen demand, biochemical oxygen demand, electrical conductivity, and ammonia nitrogen. Some, like chlorophyll-a and coloured dissolved organic matter, have optical properties detectable with RGB cameras (Goddijn and White, 2006), while non-optical parameters, like total phosphorus, can be remotely sensed by leveraging their relationship with optically active parameters, such as chlorophyll-a (Niu et al., 2021).

Furthermore, RGB cameras are effective in detecting floating materials, plumes, foam, or oil spills, with spatial image resolution matching object dimensions being the only limitation. Feature detection and labelling algorithms provide valuable insights into material density and distribution, aiding in prompt pollution event detection.

A recent review by Ramírez et al. (2023) underscores the potential of citizen science in diverse hydrological applications, especially pollution detection and water quality modelling. This section highlights the need for guidelines and protocols to ensure data meets water quality standards and is comparable across projects.

1.3.2 Turbidity as a proxy of river quality status

Turbidity detection is an important indicator of water quality and assumes great significance for environmental protection and aquatic ecosystems. It is used as a relative indicator for other physical and optical properties such as suspended sediment concentration (SSC) and total suspended solids as well as other compounds present in water such as chlorophyll, organic matter, microorganisms, algae, chemicals, and floating pollutants (Stutter et al. 2017; Tomperi et al., 2022). Since turbidity is generally closely related to these compounds, it can often be used for quantitative estimation. In inland water bodies, turbidity level and trophic state can strongly change with seasonality (Jalón-Rojas et al., 2015), soil erosion, extreme rainfall events, and farming activities (Lu et al., 2023). The growth of algae and other organisms in the summer can also cause an increase in turbidity.

Despite expensive costs for instruments and personnel, conventional in-situ monitoring techniques, using regular but not frequent sampling, return poor information to properly characterize temporal trends and spatial variability of hydrological and environmental conditions in river basins (Guo et al., 2020), usually underestimating the real loads (Gippel,1995).

In the last years, several innovations have been introduced in hydrological monitoring which exploit satellites, Unmanned Aerial Vehicles (UAV) or fixed camera systems in combination with image processing and machine learning techniques (Manfreda et al., 2018; Manfreda and Ben Dor, 2023). These methods offer the opportunity to provide large scale and detailed information on specific hydrological processes with relatively low costs. Within this context, many remote sensing applications for water quality applications have been developed (Ritchie et al., 2003; Ahmed et al., 2020), exploring the potential information coming from the water spectral signatures (Gholizadeh et al. 2016) and investigating the dynamics of riverine ecosystems (Zhao et al., 2019).

Many of these studies developed turbidity estimation algorithms using satellite products, mainly for very large rivers, reservoirs (Potes et al., 2012; Constantin et al., 2016; Garg et al., 2020; Hossain et al., 2021) and coastal areas (Dogliotti et al., 2015). Unfortunately, satellite spatial resolution can’t provide distributed estimations of water turbidity (WT) along the entire river network (Sagan et al., 2020) and the frequency of data collection is limited by satellite revisit period, usually of 5-10 days for Sentinel 2 and Landsat 8 (Jia et al., 2024). Recent studies are starting to investigate the perspective of digital cameras and low-cost optical sensors for river turbidity monitoring (Gao et al., 2022; Droujko & Molnar, 2022). However, no studies focused yet on the potential of image analysis applied in a real riverine environment. Such an application could definitively grant continuous high-frequency data, across the inland water bodies even without spatial resolution issues. Moreover, latest advances in computer vision techniques can certainly help us in extracting water quality information from images.

1.4 Overview on the experimental activities and projects

The large number of ongoing international initiatives highlights the worldwide effort aimed at developing new tools and methodologies for hydrological monitoring. In this context, we are carrying out several experimental initiatives within international projects that are useful to underline the potential of alternative techniques with practical examples. Among others, we will mention the Partnership for Research & Innovation in the Mediterranean Area (PRIMA)-funded project named "OurMED: Sustainable water storage and distribution in the Mediterranean" and "RiverWatch: a citizen-science approach to river pollution monitoring," funded by the Italian Ministry of University and Research Progetti di Rilevante Interesse Nazionale. The first project aims to explore new water-saving strategies over several demo sites distributed in different countries in the Mediterranean. Within each demo site, monitoring camera systems will be adopted to measure the water flow and turbidity. The second project is focused on the monitoring of the Sarno River, which is the most polluted river in Europe (Lofrano et al., 2015; Baldantoni et al., 2018). These examples trace the pace for a new trajectory in hydrological monitoring. These projects offer a unique opportunity to test new water monitoring ideas and tools. More details about the case studies are given in the following subsections, with the aim to identify the expected impacts associated with the ongoing activities.

1.4.1 Long term water turbidity monitoring in the Bode River

The Bode catchment is one of the meteorologically and hydrologically best-instrumented meso-scale catchments in Europe, providing high-resolution observations of water quantity and quality (Zacharias et al., 2011; Wollschläger et al., 2017). Within this catchment, the Meisdorf station has been chosen to assess the viability of camera systems for continuous water quality monitoring. In addition, targeted experiments have been conducted, inducing controlled changes in water turbidity, to test potentials of camera systems.

Preliminary results of the long-term study are given in Fig. 1.1, which describes the turbidity measurements in terms of nephelometric turbidity units (NTUs) obtained by a submerged turbidimeter and the water level gauges. Within this figure, we have selected seven significant images obtained by the trap camera which provides evidence of the relative changes of the water body colours at different levels of turbidity (Miglino et al., 2022).

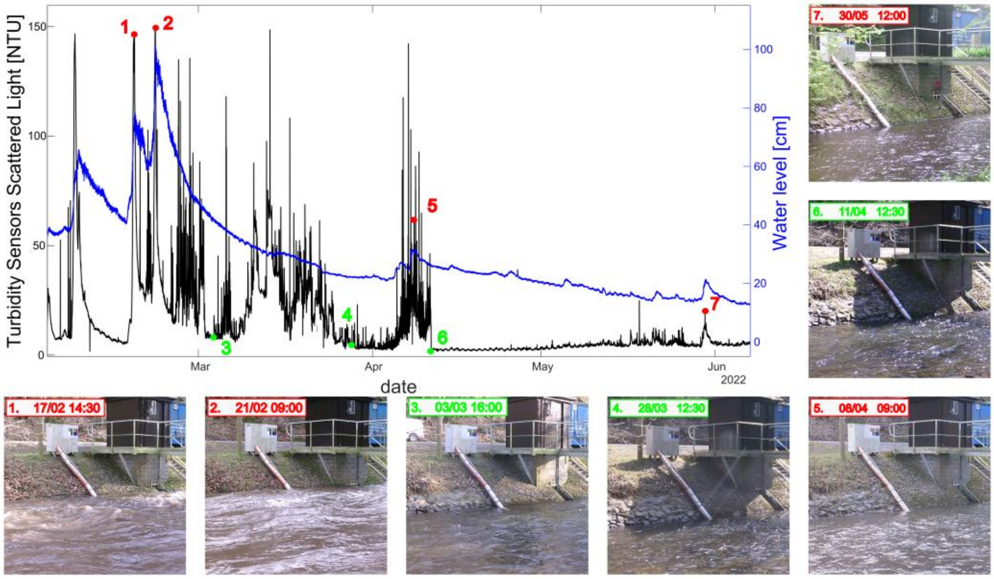

Figure 1.1: Turbidity and water level diagram from February to June 2022 with associated photographs taken at different levels of turbidity (Meisdorf station on the Selke River – tributary of the Bode River, Germany).

Our preliminary long-term monitoring data of 2022 provided a very simple installation setup: only one trap camera installed beside the river, a radiometric calibration panel installed on the other side, and a turbidimeter measurement each 15 min (Figure 1.2). The trap camera data were compared with the sensor measures, continuously collected for months. The data during the night and poor light conditions were not considered.

In Figure 1.3, we can observe a clear correspondence between the variables, especially for the two main turbidity events of February, but also conflicting results for the other low-moderate turbidity peaks.

Figure 1.2: Installation of the camera (a) and the radiometric calibration panel (b) circled in red on the site of Meisdorf station.

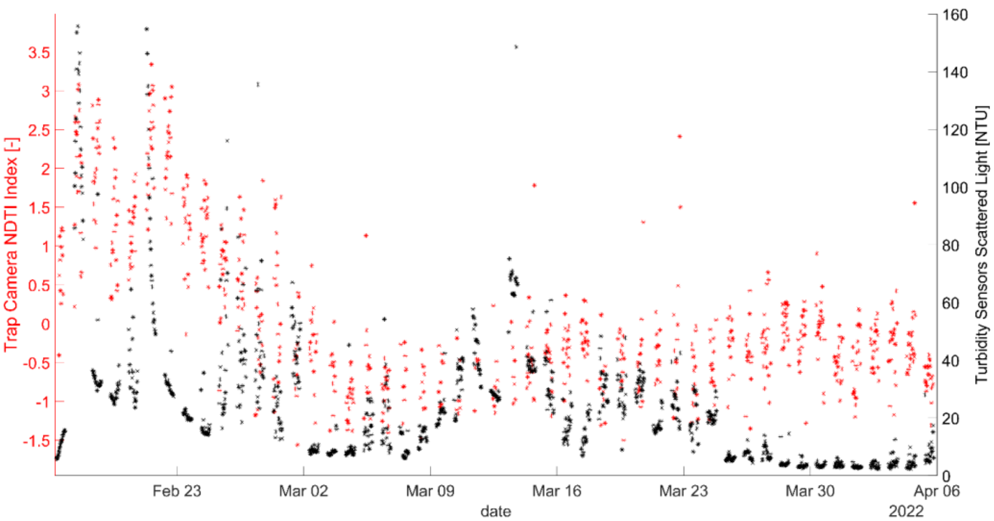

Figure 1.3: Comparison of turbidimeter measurements (in black) and trap camera NDTI index (in red) during long-term monitoring from February to April 2022

On the light of the results, we felt the need to investigate the main factors influencing the monitored process by designing a short-term experiment. This first field experience provided us the knowledge needed to design a proper experimental setup in the further studies. Short term water turbidity monitoring in the Bode River

In addition, supplementary tracer experiments were conducted by applying kaolin clay (a commonly used turbidity standard, which is a readily available, safe, and cost-effective clay mineral) upstream of the monitored river cross-section. Figure 1.2 illustrates one of these simulated events. During these events, various sensors, including optical cameras, multispectral cameras, and a drone equipped with an optical camera, were employed to capture different perspectives of the synthetic turbidity event. The data collected from these cameras were compared with the records from existing turbidity sensors at the Selke River cross-section. This figure provides an initial overview of the experimental results, emphasizing the phases of the experiment captured by RGB cameras of the trap-camera (TC) and the unmanned aereal vehicle (UAV).

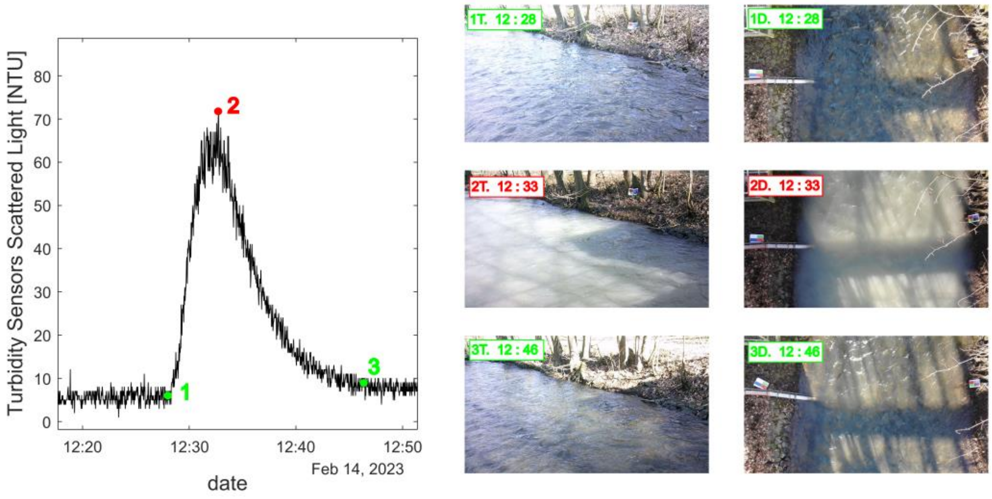

Figure 1.4: Turbidity diagram measured in February 2023 with associated photographs taken in different conditions from the TC (1T, 2T, 3T) and UAV (1D, 2D, 3D) hovering.

However, the UAS imagery offers a richer and more informative depiction of the water dynamic response, highlighting the advantages of zenithal camera positioning for comprehensive observations, but with a strong limitation for the observation time, due to the short battery life of UAS, respect to the trap camera. These short-term tracer experiments are described in detail in the following Section 2 and Section 3.

This field campaign proved invaluable for developing and refining the image processing methodology. Integrating field results allowed us to test the camera monitoring system in diverse environmental and hydrological settings. This enabled us to generalize the procedure for potential application to other water quality parameters exhibiting spectral response changes.

These experiments illuminated both the advantages and the challenges of camera systems. Though they offer a wealth of information, they can also be susceptible to significant noise and difficulties. While initial findings clearly demonstrate the system's ability to provide insights into river system trends and dynamics, several practical issues require resolution:

- Significant variations in illumination cause notable differences in spectral signatures across days and seasons.

- Changing illumination direction and resulting tree shadows alter the scene during the day.

- Flow conditions and ripples may affect the spectral signature.

- Suspended sediment colour variations can also impact the camera signal.

- Wind, human activity, or animal presence might disrupt camera positioning or even induce vibrations.

- Shallow rivers' backgrounds, particularly the cross-section, can be challenging.

These critical factors should be considered to refine camera systems' effectiveness, establishing a robust workflow for high-quality measurements. This might involve optimizing camera angles, implementing effective image filtering and calibration, securing camera stability, and providing comprehensive training for floating object detection.

1.4.2 Water quality monitoring on the Sarno River

The Sarno River is a formidable challenge: developing pioneering monitoring systems for Europe's most polluted river, situated within a complex and socioeconomically disadvantaged setting. The site has been subject to political disputes over remediation measures for a long time. It is considered the most polluted river in Europe and one of the 10 most polluted rivers in the world. The river drains a watershed area of 540 km2 densely populated with heavy agricultural and industrial activities. The distribution of different activities in the basin is clustered, which leads to strong spatial variability and temporal fluctuations of environmental conditions (Montuori et al., 2013, Cicchella et al., 2014).

Figure 1.3 shows four images of the Sarno River at Scafati in different conditions: ordinary condition, dense presence of macroplastic (polystyrene foams) and organic material, presence of plastic elements, and presence of foam on the surface.

UAS and camera images have been instrumental in capturing a comprehensive view of water quality dynamics, encompassing factors such as turbidity levels, plastic presence, and pollutant transport. Notably, images offer a distinct advantage in their ability to reveal the spatial distribution of pollution. This capability enables us to precisely identify the sources of specific contaminants and accurately depict the processes of intermingling between polluted and clean water. In this context, Figs. 1.4 and 1.5 provide a detailed representation of the mixing of contaminated water. Figure 1.4 illustrates the confluence of the Nocerino tributary into the Sarno River using thermal cameras, while Fig. 1.5 depicts the outlet of the Sarno River using a turbidity index.

Figure 1.5: Examples of images taken on the Sarno River at Scafati (Italy) where the presence of suspended material is clearly visible: (a) ordinary condition; (b) dense presence of macroplastic (polystyrene foams) and organic material; (c) presence of plastic elements; (d) presence of foam on the surface.

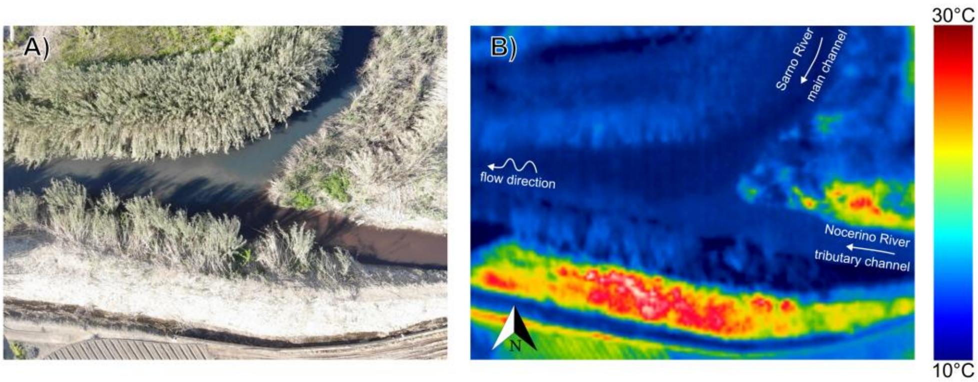

Figure 1.6: Example of UAS-based imagery obtained with (a) an RGB and (b) a thermal camera at the confluence of the Nocerino River and the Sarno River. The image shows a clear flow of pollutants coming from the right tributary.

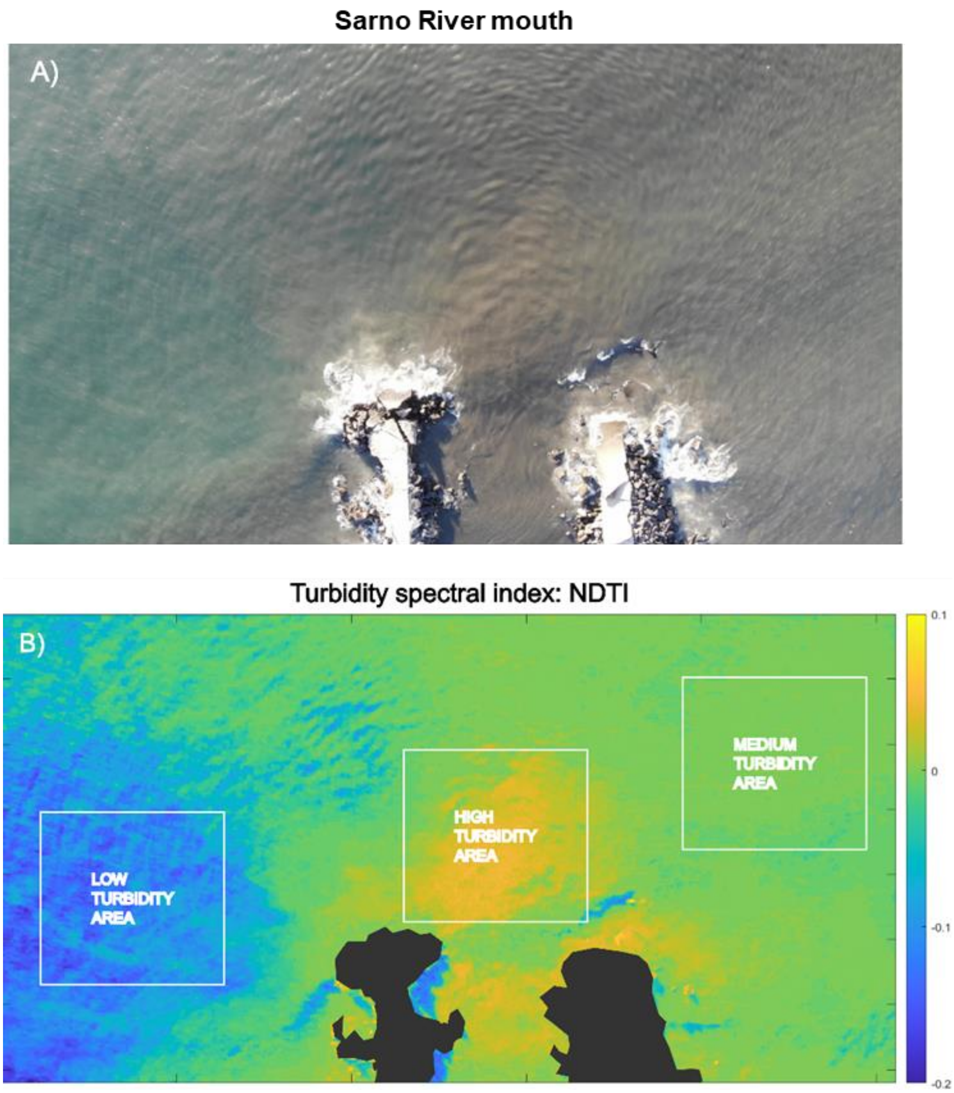

Figure 1.7: Outlet of the Sarno River: (a) RGB UAS image, (b) normalized difference turbidity index, NDTI = (R − G) / (R + G) obtained as the ratio between the red (R) and green (G) bands.

Figure 1.4(a) presents an RGB aerial image of the confluence of the Nocerino tributary and the Sarno River. The image clearly shows the distinct chromatic differences between the two water bodies, confirmed by the thermal image in Fig. 1.4(b). The higher temperature visible in the Nocerino tributary suggests a substantial inflow of sewer water, likely causing the thermal contrast.

Downstream from the confluence, the river's turbidity noticeably increases, serving as a strong indicator of aquatic ecosystem pollution. As the river approaches its mouth at the Tyrrhenian Sea, a clear blending of this concentrated pollutant plume with seawater becomes evident. This mixing process is vividly illustrated in Fig. 1.5(b), where the Normalized Difference Turbidity Index (NDTI) derived from RGB UAS imagery visually depicts this phenomenon.

The activities along the Sarno River serve as an ideal source of new training data. Leveraging this data will contribute to optimizing the utilization of a tool that has rapidly evolved into an indispensable and versatile resource for a multitude of applications.

In order to improve the training of these algorithms, there is a need for a large amount of training data which could be provided by any volunteer. With this aim, we are promoting the construction of an image repository, collecting images of rivers with the presence of different pollutants or floating materials. This activity will be carried out within the project RiverWatch and it is possible to contribute to this data collection effort using the following link: https://forms.gle/WHvGvqQc6p3zdEuN9.

1.4.3 Ongoing projects' goals

The challenges of hydrological monitoring, encompassing issues such as data scarcity, spatial and temporal variability, and the growing demand for water resource monitoring, are exacerbated by climate change, which will have significant environmental and socioeconomic impacts. Our analysis emphasizes the need for high-resolution observations in this rapidly evolving environment, where river dynamics and water quality undergo constant changes. Developing new tools capable of providing a holistic picture of a river's state is crucial for securing water supply and ensuring environmental safety.

In this context, the international community is actively exploring the potential of innovative approaches and technologies, including satellite-based technologies, UASs, camera systems, big data analytics, sensor networks, and citizen science. The integration of multiple data sources and the utilization of innovative approaches offer new prospects for addressing data scarcity, enhancing spatial and temporal resolution, and advancing our comprehension of complex hydrological processes.

Combining remote sensing data with machine learning holds great potential for creating more comprehensive river monitoring systems (Maier & Keller, 2019; Arias-Rodriguez et al., 2020). Global experiments across diverse basins highlight both challenges and advantages of this approach. We have actively participated in and developed initiatives showcasing the convenience and wide applicability of remote sensing coupled with image processing techniques. These experiences lay the groundwork for a new generation of sensors – from RGB to hyperspectral and thermal – unlocking the power of image processing to extract diverse hydraulic, hydromorphological, and water-quality-related parameters.

Reviewing existing activities and research reveals critical limitations and challenges in using innovative technologies for river monitoring:

- Developing systems flexible enough to handle diverse hydraulic, environmental, and climatic conditions remains a key challenge. Different river cross-sections within the same basin can have unique characteristics due to upstream features or local specifics. This requires testing in diverse environments and sharing experiences and data openly with the research community.
- Although satellites are powerful tools for hydrological and hydromorphological monitoring, their limited spatial resolution often hinders their use in narrower river networks worldwide. Proximity sensors, however, offer a promising alternative to overcome this limitation.
- Image-based techniques are susceptible to local factors like illumination, surrounding environment, tree shadows, and cross-section background. Developing standardized pre-processing techniques is crucial to ensure consistent data quality and maximize information in each survey or measurement.

- Individual pollutants and their combination within a specific location can complicate the interpretation of spectral signatures in any type of imagery, posing a significant challenge that needs to be addressed.
- The substantial volume of data collected by these sensors may lead to information overload, which may not always be useful for specific purposes. Consequently, there is a need to synthesize the information and develop meaningful metrics capable of retaining essential data.
- New techniques based on camera use and citizen participation can be susceptible to significant disturbances and procedural errors, potentially degrading the quality of the collected information. Therefore, establishing standardized protocols and sustainable systems for using such methods is critical.

There are still many issues that require further investigation to bring these methods to operational use. However, numerous opportunities exist for advancing hydrological monitoring using these innovative techniques. Here, we highlight some of the key opportunities:

- Affordable commercial devices: The use of image-based techniques could lead to the development of cost-effective commercial devices that can be integrated into sensor networks, even in remote regions around the world.
- Integration of crowd-sourced data: The integration of crowd-sourced data with image processing appears to be a natural progression for the evolution of new monitoring techniques.
- Citizen-friendly tools: Creating user-friendly tools that could potentially be used on smartphones by the public may expand the overall number of hydrological sensors. This could have significant environmental benefits by fostering a community engaged in river monitoring, raising awareness about the state of aquatic ecosystems, and working towards their protection. Additionally, this approach could address some typical limitations often

encountered in traditional techniques, such as theft, vandalism, reliance on a power supply, and high acquisition and running costs.

- Multipurpose systems: Leveraging these innovative tools can yield a wealth of information regarding watercourse dynamics that surpasses the capabilities of traditional methods. Such data can be invaluable in bolstering the management of river systems, offering a comprehensive depiction of the river's current condition.

Even with limitations and advantages considered, a critical challenge remains shifting from qualitative to quantitative assessments. This transition stands as arguably the biggest hurdle on our journey forward.

References

Ahmed, U., Mumtaz, R., Anwar, H., Mumtaz, S., & Qamar, A. M.: Water quality monitoring: from conventional to emerging technologies, Water Supply, 20(1), 28-45, https://doi.org/10.2166/ws.2019.144, 2020.

Albertini, C., Gioia, A., Iacobellis, V., Manfreda, S., 2022, Detection of Surface Water and Floods with Multispectral Satellites. Remote Sensing, 14, 6005.

Alilou, H., Nia, A.M., Saravi, M.M., Salajegheh, A., Han, D. and Enayat, B.B., 2019. A novel approach for selecting sampling points locations to river water quality monitoring in data-scarce regions. Journal of Hydrology, 573, pp.109-122.

Allamano, P., Croci, A., & Laio, F. (2015). Toward the camera rain gauge. Water Resources Research, 51(3), 1744-1757.

Arias-Rodriguez, L.F., Duan, Z., Sepúlveda, R., Martinez-Martinez, S.I. and Disse, M., 2020. Monitoring water quality of valle de bravo reservoir, mexico, using entire lifespan of meris data and machine learning approaches. Remote Sensing, 12(10), p.1586.

Baldantoni, D., Bellino, A., Lofrano, G., Libralato, G., Pucci, L. and Carotenuto, M., 2018. Biomonitoring of nutrient and toxic element concentrations in the Sarno River through aquatic plants. Ecotoxicology and Environmental Safety, 148, pp.520-527.

Balsamo, G., Agusti-Parareda, A., Albergel, C., Arduini, G., Beljaars, A., Bidlot, J., Blyth, E., Bousserez, N., Boussetta, S., Brown, A. and Buizza, R., 2018. Satellite and in situ observations for advancing global Earth surface modelling: A Review. Remote Sensing, 10(12), p.2038.

Baraniello, V. R., Persechino, G., Angelino, C. V., and Tufano, F., 2021. The Application of High-Altitude Pseudo-Satellites for a Rapid Disaster Response. In 2021 IEEE International Geoscience and Remote Sensing Symposium IGARSS (pp. 8400-8403). IEEE.

Bhateria, R. and Jain, D., 2016. Water quality assessment of lake water: a review.

Chen, L. and Wang, L., 2018. Recent advance in earth observation big data for hydrology. Big Earth Data, 2(1), pp.86-107.

Cicchella, D., Giaccio, L., Lima, A., Albanese, S., Cosenza, A., Civitillo, D. and De Vivo, B., 2014. Assessment of the topsoil heavy metals pollution in the Sarno River basin, south Italy. Environmental earth sciences, 71, pp.5129-5143.

Coney, J., Pickering, B., Dufton, D., Lukach, M., Brooks, B. and Neely III, R.R., 2022. How useful are crowdsourced air temperature observations? An assessment of Netatmo stations and quality control schemes over the United Kingdom. Meteorological Applications, 29(3), p.e2075.

de Vos, L.W., Leijnse, H., Overeem, A. and Uijlenhoet, R., 2019. Quality control for crowdsourced personal weather stations to enable operational rainfall monitoring. Geophysical Research Letters, 46(15), pp.8820-8829.

Demarchi, L., Bizzi, S. and Piégay, H., 2017. Regional hydromorphological characterization with continuous and automated remote sensing analysis based on VHR imagery and low-resolution LiDAR data. Earth Surface Processes and Landforms, 42(3), pp.531-551.

Dogliotti, A. I., Ruddick, K. G., Nechad, B., Doxaran, D., & Knaeps, E.: A single algorithm to retrieve turbidity from remotely sensed data in all coastal and estuarine waters, Remote sensing of environment, 156, 157-168, https://doi.org/10.1016/j.rse.2014.09.020, 2015

ESA, 2023. Mission Navigator [online]. Available from: https://www.esa.int/ESA/Our_Missions [Accessed 13 October 2023].

Etter, S., Strobl, B., Seibert, J. and van Meerveld, H.I., 2020. Value of crowd-based water level class observations for hydrological model calibration. Water Resources Research, 56(2), p.e2019WR026108.

Gao, M., Li, J., Wang, S., Zhang, F., Yan, K., Yin, Z., ... & Shen, W.: Smartphone–Camera–Based Water Reflectance Measurement and Typical Water Quality Parameter Inversion, Remote Sensing, 14(6), 1371, https://doi.org/10.3390/rs14061371, 2022.

GEWEX, 2018. Gewex. Available from: https://www.gewex.org/ [Accessed 13 October 2023].

Gholizadeh, M.H., Melesse, A.M. and Reddi, L., 2016. A comprehensive review on water quality parameters estimation using remote sensing techniques. Sensors, 16(8), p.1298.

Gippel, C. J.: Potential of turbidity monitoring for measuring the transport of suspended solids in streams, Hydrological processes, 9(1), 83-97, https://doi.org/10.1002/hyp.3360090108, 1995.

Gonzalo, J., López, D., Domínguez, D., García, A., and Escapa, A., 2018. On the capabilities and limitations of high altitude pseudo-satellites. Progress in Aerospace Sciences, 98, 37-56

Graf, M., El Hachem, A., Eisele, M., Seidel, J., Chwala, C., Kunstmann, H. and Bárdossy, A., 2021. Rainfall estimates from opportunistic sensors in Germany across spatio-temporal scales. Journal of Hydrology: Regional Studies, 37, p.100883.

Guo, D., Lintern, A., Webb, J. A., Ryu, D., Bende-Michl, U., Liu, S., & Western, A. W.: A data-based predictive model for spatiotemporal variability in stream water quality, Hydrology and Earth System Sciences, 24(2), 827-847, https://doi.org/10.5194/hess-24-827-2020, 2020.

Hannah, D.M., Abbott, B.W., Khamis, K., Kelleher, C., Lynch, I., Krause, S. and Ward, A.S., 2022. Illuminating the 'invisible water crisis' to address global water pollution challenges. Hydrological Processes, 36(3).

Harley, M.D., Kinsela, M.A., Sánchez-García, E. and Vos, K., 2019. Shoreline change mapping using crowd-sourced smartphone images. Coastal Engineering, 150, pp.175-189.

Hossain, A. A., Mathias, C., & Blanton, R.: Remote sensing of turbidity in the Tennessee River using Landsat 8 satellite, Remote Sensing, 13(18), 3785, https://doi.org/10.3390/rs13183785, 2021.

Hsu, W.L., Liao, H.M., Jeng, B.S. and Fan, K.C., 2003, October. Real-time vehicle tracking on highway. In Proceedings of the 2003 IEEE International Conference on Intelligent Transportation Systems (Vol. 2, pp. 909-914). IEEE.

IAHS, 2023. HELPING Working Groups [online]. IAHS. Available from: https://iahs.info/Initiatives/Topic-for-the-Next-IAHS-decade/helping-working-groups/ [Accessed 12 October 2023].

Jalón-Rojas, I., Schmidt, S., & Sottolichio, A.: Turbidity in the fluvial Gironde Estuary (southwest France) based on 10-year continuous monitoring: sensitivity to hydrological conditions, Hydrology and Earth System Sciences, 19(6), 2805-2819, https://doi.org/10.5194/hess-19-2805-2015, 2015.

James, M.R., Chandler, J.H., Eltner, A., Fraser, C., Miller, P.E., Mills, J.P., Noble, T., Robson, S. and Lane, S.N., 2019. Guidelines on the use of structure-from-motion photogrammetry in geomorphic research. Earth Surface Processes and Landforms, 44(10), pp.2081-2084.

Jiang, S., Babovic, V., Zheng, Y. and Xiong, J., 2019. Advancing opportunistic sensing in hydrology: A novel approach to measuring rainfall with ordinary surveillance cameras. Water Resources Research, 55(4), pp.3004-3027.

Johnson, E.D. and Cowen, E.A., 2017. Remote determination of the velocity index and mean streamwise velocity profiles. Water Resources Research, 53(9), pp.7521-7535.

Kavian, A., Mohammadi, M., Cerda, A., Fallah, M. and Abdollahi, Z., 2018. Simulated raindrop's characteristic measurements. A new approach of image processing tested under laboratory rainfall simulation. Catena, 167, pp.190-197.

Kirchner, J.W., 2006. Getting the right answers for the right reasons: Linking measurements, analyses, and models to advance the science of hydrology. Water resources research, 42(3).

Koparan, C., Koc, A.B., Privette, C.V. and Sawyer, C.B., 2018. In situ water quality measurements using an unmanned aerial vehicle (UAV) system. Water, 10(3), p.264.

Koparan, C., Koc, A.B., Sawyer, C. and Privette, C., 2020. Temperature profiling of waterbodies with a UAV-integrated sensor subsystem. Drones, 4(3), p.35.

Krüger, R., Karrasch, P. and Eltner, A., 2023. Calibrating low-cost rain gauge sensors for their applications in IoT infrastructures to densify environmental monitoring networks. Geoscientific Instrumentation, Methods and Data Systems Discussions, 2023, pp.1-20.

Lee, I. and Lee, K., 2015. The Internet of Things (IoT): Applications, investments, and challenges for enterprises. Business horizons, 58(4), pp.431-440.

Lewis, Q.W. and Rhoads, B.L., 2018. LSPIV measurements of two-dimensional flow structure in streams using small unmanned aerial systems: 2. Hydrodynamic mapping at river confluences. Water Resources Research, 54(10), pp.7981-7999.

Livoroi, A.H., Conti, A., Foianesi, L., Tosi, F., Aleotti, F., Poggi, M., Tauro, F., Toth, E., Grimaldi, S. and Mattoccia, S., 2021. On the deployment of out-of-the-box embedded devices for self-powered river surface flow velocity monitoring at the edge. Applied Sciences, 11(15), p.7027.

Lofrano, G., Libralato, G., Acanfora, F.G., Pucci, L. and Carotenuto, M., 2015. Which lesson can be learnt from a historical contamination analysis of the most polluted river in Europe?. Science of the Total Environment, 524, pp.246-259.

Maier, P.M. and Keller, S., 2019, September. Application of different simulated spectral data and machine learning to estimate the chlorophyll a concentration of several inland waters. In 2019 10th Workshop on Hyperspectral Imaging and Signal Processing: Evolution in Remote Sensing (WHISPERS) (pp. 1-5). IEEE.

Manfreda, S. and Ben Dor, E. eds., 2023. Unmanned Aerial Systems for Monitoring Soil, Vegetation, and Riverine Environments.

Manfreda, S., McCabe, M.F., Miller, P.E., Lucas, R., Pajuelo Madrigal, V., Mallinis, G., Ben Dor, E., Helman, D., Estes, L., Ciraolo, G. and Müllerová, J., 2018. On the use of unmanned aerial systems for environmental monitoring. Remote sensing, 10(4), p.641.

Mapiam, P.P., Methaprayun, M., Bogaard, T., Schoups, G. and Ten Veldhuis, M.C., 2022. Citizen rain gauges improve hourly radar rainfall bias correction using a two-step Kalman filter. Hydrology and Earth System Sciences, 26(3), pp.775-794.

Marino, P., Roman Quintero, D.C., Santonastaso, G.F. and Greco, R., 2023. Prototype of an IoT-based low-cost sensor network for the hydrological monitoring of landslide-prone areas. Sensors, 23(4), p.2299.

McCabe, M.F., Rodell, M., Alsdorf, D.E., Miralles, D.G., Uijlenhoet, R., Wagner, W., Lucieer, A., Houborg, R., Verhoest, N.E., Franz, T.E. and Shi, J., 2017. The future of Earth observation in hydrology. Hydrology and earth system sciences, 21(7), pp.3879-3914.

Meijer, L.J., Van Emmerik, T.H.M., Van Der Ent, R., Schmidt, C. and Lebreton, L., 2021. More than 1000 rivers account for 80% of global riverine plastic emissions into the ocean. Science Advances, 7(18), p.eaaz5803.

Metzger, J.C., Wutzler, T., Dalla Valle, N., Filipzik, J., Grauer, C., Lehmann, R., Roggenbuck, M., Schelhorn, D., Weckmüller, J., Küsel, K. and Totsche, K.U., 2017. Vegetation impacts soil water content patterns by shaping canopy water fluxes and soil properties. Hydrological processes, 31(22), pp.3783-3795.

Miglino, D., Jomaa, S., Rode, M., Isgro, F. and Manfreda, S., 2022. Monitoring Water Turbidity Using Remote Sensing Techniques. Environmental Sciences Proceedings, 21(1), p.63.

Montanari, A., Young, G., Savenije, H.H.G., Hughes, D., Wagener, T., Ren, L.L., Koutsoyiannis, D., Cudennec, C., Toth, E., Grimaldi, S. and Blöschl, G., 2013. “Panta Rhei—everything flows”: change in hydrology and society—the IAHS scientific decade 2013–2022. Hydrological Sciences Journal, 58(6), pp.1256-1275.

Montuori, P., Lama, P., Aurino, S., Naviglio, D. and Triassi, M., 2013. Metals loads into the Mediterranean Sea: estimate of Sarno River inputs and ecological risk. Ecotoxicology, 22, pp.295-307.

Nardi, F., Cudennec, C., Abrate, T., Allouch, C., Annis, A., Assumpcao, T., Aubert, A.H., Berod, D., Braccini, A.M., Buytaert, W. and Dasgupta, A., 2022. Citizens AND HYdrology (CANDHY): conceptualizing a transdisciplinary framework for citizen science addressing hydrological challenges. Hydrological Sciences Journal, 67(16), pp.2534-2551.

NASA, 2023. Featured Missions & Projects - Earth Sciences Division (610) [online]. Washington, NASA. Available from: https://science.gsfc.nasa.gov/sed/index.cfm?fuseaction=projects.featured&navOrgCode=610&navTab=nav_about_us [Accessed 13 October 2023].

Niu, C., Tan, K., Jia, X. and Wang, X., 2021. Deep learning based regression for optically inactive inland water quality parameter estimation using airborne hyperspectral imagery. Environmental Pollution, 286, p.117534.

Outram, F.N., Lloyd, C.E.M., Jonczyk, J., Benskin, C.M.H., Grant, F., Perks, M.T., Deasy, C., Burke, S.P., Collins, A.L., Freer, J. and Haygarth, P.M., 2014. High-frequency monitoring of nitrogen and phosphorus response in three rural catchments to the end of the 2011–2012 drought in England. Hydrology and earth system sciences, 18(9), pp.3429-3448.

Pereira, B., Medeiros, P., Francke, T., Ramalho, G., Foerster, S. and De Araújo, J.C., 2019. Assessment of the geometry and volumes of small surface water reservoirs by remote sensing in a semi-arid region with high reservoir density. Hydrological Sciences Journal, 64(1), pp.66-79.

Perks, M.T., 2020. KLT-IV v1. 0: Image velocimetry software for use with fixed and mobile platforms. Geoscientific Model Development, 13(12), pp.6111-6130.

Perumal, T., Sulaiman, M.N. and Leong, C.Y., 2015, October. Internet of Things (IoT) enabled water monitoring system. In 2015 IEEE 4th Global Conference on Consumer Electronics (GCCE) (pp. 86-87). IEEE.

Peters-Lidard, C.D., Clark, M., Samaniego, L., Verhoest, N.E., Van Emmerik, T.H.M., Uijlenhoet, R., Achieng, K., Franz, T.E. and Woods, R., 2017. Scaling, similarity, and the fourth paradigm for hydrology. Hydrology and earth system sciences, 21(7), pp.3701-3713.

Piégay, H., Arnaud, F., Belletti, B., Bertrand, M., Bizzi, S., Carbonneau, P., Dufour, S., Liébault, F., Ruiz-Villanueva, V. and Slater, L., 2020. Remotely sensed rivers in the Anthropocene: State of the art and prospects. Earth Surface Processes and Landforms, 45(1), pp.157-188.

Poghosyan, A., & Golkar, A., 2017, CubeSat evolution: Analyzing CubeSat capabilities for conducting science missions. Progress in Aerospace Sciences, 88, 59-83.

Ramírez, S.B., van Meerveld, I. and Seibert, J., 2023. Citizen science approaches for water quality measurements. Science of the Total Environment, p.165436.

Ritchie, J. C., Zimba, P. V., & Everitt, J. H.: Remote sensing techniques to assess water quality, Photogrammetric engineering & remote sensing, 69(6), 695-704, https://doi.org/10.14358/PERS.69.6.695, 2003.

Rode, M., Wade, A.J., Cohen, M.J., Hensley, R.T., Bowes, M.J., Kirchner, J.W., Arhonditsis, G.B., Jordan, P., Kronvang, B., Halliday, S.J. and Skeffington, R.A., 2016. Sensors in the stream: the high-frequency wave of the present.

Rodríguez-Iturbe, I., Isham, V., Cox, D.R., Manfreda, S. and Porporato, A., 2006. Space-time modeling of soil moisture: Stochastic rainfall forcing with heterogeneous vegetation. Water resources research, 42(6).

Ross, A., & Chang, H., 2020. Socio-hydrology with hydrosocial theory: two sides of the same coin?. Hydrological Sciences Journal, 65(9), 1443-1457.

Sagan, V., Peterson, K. T., Maimaitijiang, M., Sidike, P., Sloan, J., Greeling, B. A., ... & Adams, C.: Monitoring inland water quality using remote sensing: Potential and limitations of spectral indices, bio-optical simulations, machine learning, and cloud computing, Earth-Science Reviews, 205, 103187, https://doi.org/10.1016/j.earscirev.2020.103187, 2020.

Seibert, J., Strobl, B., Etter, S., Hummer, P. and van Meerveld, H.J., 2019. Virtual staff gauges for crowd-based stream level observations. Frontiers in Earth Science, 7, p.70.

Sergeant, C.J. and Nagorski, S., 2015. The implications of monitoring frequency for describing riverine water quality regimes. River Research and Applications, 31(5), pp.602-610.

Sermet, Y., Villanueva, P., Sit, M. A., & Demir, I., 2020. Crowdsourced approaches for stage measurements at ungauged locations using smartphones. Hydrological Sciences Journal, 65(5), 813-822.

Shi, J., Dong, X., Zhao, T., Du, Y., Liu, H., Wang, Z., Zhu, D., Ji, D., Xiong, C. and Jiang, L., 2016, July. The water cycle observation mission (WCOM): Overview. In 2016 IEEE International Geoscience and Remote Sensing Symposium (IGARSS) (pp. 3430-3433). IEEE.

Strelnikova, D., Perks, M.T., Dal Sasso, S.F. and Pizarro, A., 2023. River flow monitoring with unmanned aerial system. In Unmanned Aerial Systems for Monitoring Soil, Vegetation, and Riverine Environments (pp. 231-269). Elsevier.

Strobl, B., Etter, S., van Meerveld, I. and Seibert, J., 2019. The CrowdWater game: A playful way to improve the accuracy of crowdsourced water level class data. PLoS One, 14(9), p.e0222579.

Stutter, M., Dawson, J. J., Glendell, M., Napier, F., Potts, J. M., Sample, J., ... & Watson, H.: Evaluating the use of in-situ turbidity measurements to quantify fluvial sediment and phosphorus concentrations and fluxes in agricultural streams, Science of the Total Environment, 607, 391-402, https://doi.org/10.1016/j.scitotenv.2017.07.013, 2017.

Taramelli, A., Tornato, A., Magliozzi, M.L., Mariani, S., Valentini, E., Zavagli, M., Costantini, M., Nieke, J., Adams, J. and Rast, M., 2020. An interaction methodology to collect and assess user-driven requirements to define potential opportunities of future hyperspectral imaging sentinel mission. Remote Sensing, 12(8), p.1286.

Tauro, F., Selker, J., Van De Giesen, N., Abrate, T., Uijlenhoet, R., Porfiri, M., Manfreda, S., Caylor, K., Moramarco, T., Benveniste, J. and Ciraolo, G., 2018a. Measurements and Observations in the XXI century (MOXXI): innovation and multi-disciplinarity to sense the hydrological cycle. Hydrological sciences journal, 63(2), pp.169-196.

Tomperi, J., Isokangas, A., Tuuttila, T., & Paavola, M.: Functionality of turbidity measurement under changing water quality and environmental conditions, Environmental technology, 43(7),1093-1101, https://doi.org/10.1080/09593330.2020.1815860, 2022.

Tosi, F., Rocca, M., Aleotti, F., Poggi, M., Mattoccia, S., Tauro, F., Toth, E. and Grimaldi, S., 2020. Enabling image-based streamflow monitoring at the edge. Remote Sensing, 12(12), p.2047.

van Lieshout, C., van Oeveren, K., van Emmerik, T.H.M. and Postma, E., 2020. Automated river plastic monitoring using deep learning and cameras. Earth and space science, 7(8), p.e2019EA000960.

Wang, W., Guo, L., Wu, Y. J., Goh, M., & Wang, S.: Content-oriented or persona-oriented? A text analytics of endorsement strategies on public willingness to participate in citizen science, Information Processing & Management, 59(2), 102832, 2022.

Wang, X. and Yang, W., 2019. Water quality monitoring and evaluation using remote sensing techniques in China: A systematic review. Ecosystem Health and Sustainability, 5(1), pp.47-56.

Waterbase - Water Quality ICM, 2022. European Environment Agency. https://www.eea.europa.eu/en/datahub/datahubitem-view/fbf3717c-cd7b-4785-933a-d0cf510542e1 (Accessed: October 2023)

Wollschläger, U., Attinger, S., Borchardt, D., Brauns, M., Cuntz, M., Dietrich, P., Fleckenstein, J.H., Friese, K., Friesen, J., Harpke, A. and Hildebrandt, A., 2017. The Bode hydrological observatory: a platform for integrated, interdisciplinary hydro-ecological research within the TERENO Harz/Central German Lowland Observatory. Environmental Earth Sciences, 76, pp.1-25.

Zacharias, S., Bogena, H., Samaniego, L., Mauder, M., Fuß, R., Pütz, T., Frenzel, M., Schwank, M., Baessler, C., Butterbach-Bahl, K. and Bens, O., 2011. A network of terrestrial environmental observatories in Germany. Vadose zone journal, 10(3), pp.955-973.

Zanella, A., Zubelzu, S., Bennis, M., Capuzzo, M. and Tarolli, P., 2023, January. Internet of Things for Hydrology: Potential and Challenges. In 2023 18th Wireless On-Demand Network Systems and Services Conference (WONS) (pp. 114-121). IEEE.

Zhang, C., Yan, J., Li, C., Rui, X., Liu, L. and Bie, R., 2016, October. On estimating air pollution from photos using convolutional neural network. In Proceedings of the 24th ACM international conference on Multimedia (pp. 297-301).

Zhao, C., Pan, T., Dou, T., Liu, J., Liu, C., Ge, Y., ... & Lim, R.: Making global river ecosystem health assessments objective, quantitative and comparable, Science of the total environment, 667, 500-510, https://doi.org/10.1016/j.scitotenv.2019.02.379, 2019.

2 Image Processing for Continuous River Turbidity Monitoring: A Full-Scale Experimental Approach

This section explores the use of an image-based monitoring procedure developed for river turbidity estimation. It was carried out within a real river where an artificial perturbation of the water turbidity has been used to find the optimal configuration for camera systems, the best performing band and range of applicability of the procedure. To follow, a short introduction with the background used, then the field experiment and methods are illustrated and finally the experimental results are presented.

2.1 RGB image acquisition and interpretation

The use of digital cameras in river monitoring activities can increase our knowledge of the real status of water bodies, solving the above-mentioned cost and data resolution problems of the existing techniques. The challenge of image-based procedures is the proper red, green, and blue (RGB) signal interpretation and processing. Goddijn et al. (2009) affirm that cameras can be seen as three-band radiometers, able to measure the water-leaving spectral response. The actual water upwelling light R_w that reaches the camera lens, schematically shown in Figure 2.1, is the sum of various reflectance components of the suspended particles (R_s), the riverbed background (R_b) and the water itself. One component could prevail over the others, depending on the variability of hydrological (water level, flow velocity, etc.) and environmental (suspended solids concentration, floating pollutants, etc.) characteristics of the river. Digital cameras receive these inputs and return a signal in terms of RGB pixel intensity values.

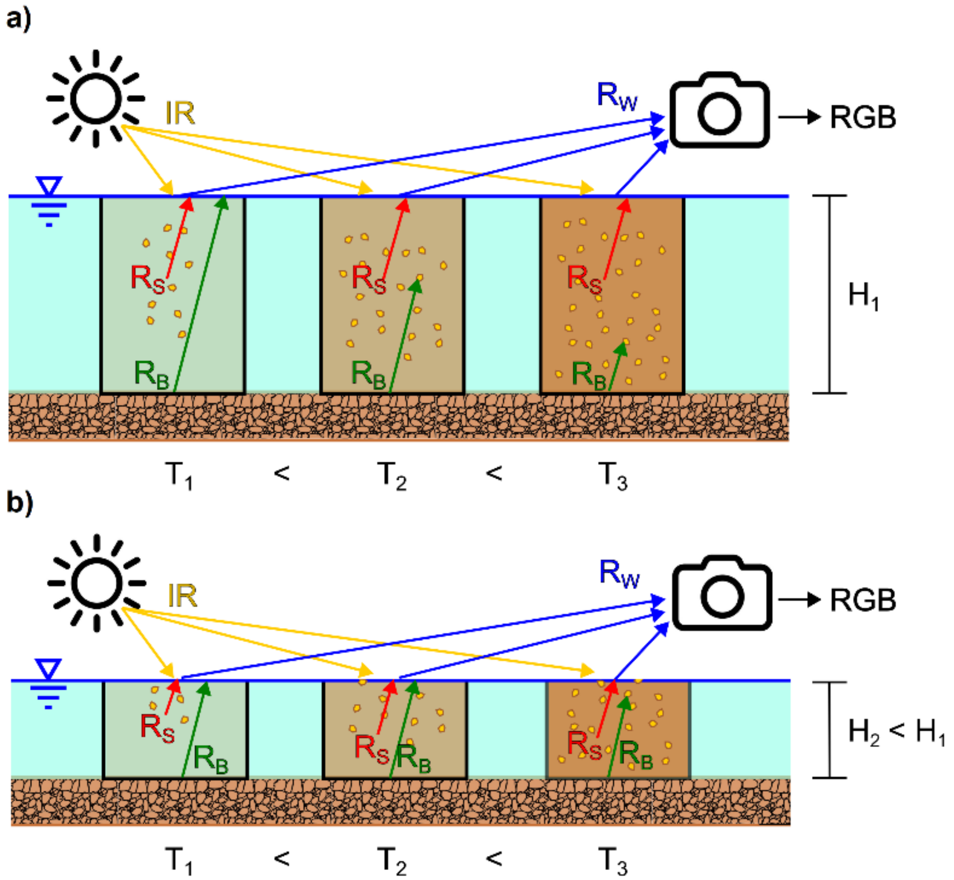

Figure 2.1: Light behaviour within shallow (b) and non-shallow water (a): The solar irradiance (IR) passes through the water, whose reflectance (Rw) is influenced by the background (Rb) and suspended particles (Rs) presence, by varying the water level (H). Finally, the total water reflectance (Rw) signal is caught by the digital camera that produces an image with different pixel intensities of red, green and blue values (RGB).

The effect of water level and turbidity concentration on the riverbed component R_b of the total water upwelling light can be schematized as shown in Figure 2.2.
In particular, for shallow water (Figure 2.1b) the riverbed is visible for higher turbidity concentration, respect to non-shallow water condition. As a result, the R_b component is more relevant and, if neglected, it can significantly affect the evaluation of the water reflectance R_w.

Another factor is the riverbed sediments characteristics. The larger the difference between the riverbed and the actual water reflectances, the more the Rw is affected by the visible background (BG). This gap depends mainly on the river BG sediments reflectance values.

We can observe that the correlation between turbidity and water reflectance is valid only in the range of turbidity values where the BG becomes substantially not visible. In addition, we can't correlate extremely high turbidity concentrations over the water reflectance saturation level $R_{w\ max}$ (Luo et al., 2018).

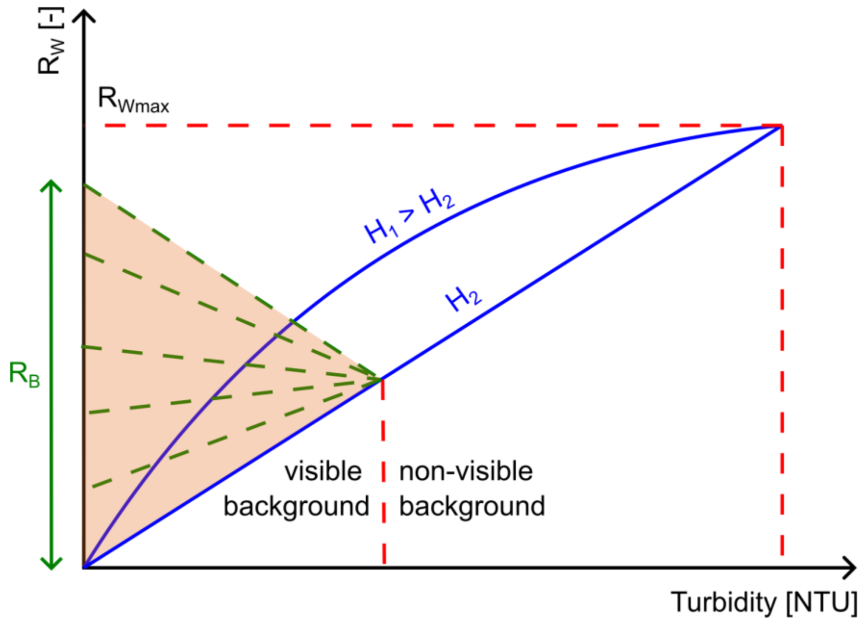

Figure 2.2: Schematization of water reflectance R_w and riverbed reflectance R_b behaviours under varying turbidity and water levels.

2.2 Turbidity image-based measurements

In the literature, there is a robust relationship between digital camera output and water quality indicators. Each of these methods requires specific solutions to provide trustable results based on the absolute water color estimation under changing light conditions. For instance, Goddijn and White (2006) fixed a pipe around the camera lens to avoid external reflections for adjusting the image data collection. Leeuw and Boss (2018) developed an innovative smartphone app called "Hydrocolor", using images of the sky and a grey card nearby the camera's view field as radiometric references for turbidity estimation from the pictures of the water. Nevertheless, the reliability of their results strongly depends on the quality of the unsupervised image data coming from the citizens and the environmental conditions, resulting in inaccurate estimates for water surface roughness and changing weather conditions. More recently, Ghorbani et al. (2020) provided a continuous monitoring camera tool for suspended sediment concentrations (SSC) and turbidity, by using image analytics methods and machine learning techniques. They found evidence of correlation between SSC and camera images in their experiments under laboratory-controlled conditions.

In real riverine environments there are many more variables to consider. The image reflectance can be strongly influenced by several factors regarding river flow and light conditions variability. Moreover, different bands could provide several information about the water status, both considering single bands and their combinations. Nechad et al. (2010) demonstrated that single bands in the red and NIR (Near-Infrared) spectral ranges give a robust outcome in mapping total suspended matter in coastal turbid waters using several satellite data sources. However, the choice of single bands or their combination is dictated by the concentration of the suspended solids and the type of floating pollutants, as well as water depth and riverbed BG. In addition, the accuracy of the estimates is certainly influenced by camera positioning and orientation with respect to the examined river section. Our analysis involved the installation of a trap camera (TC), a multispectral camera (MSC), and an Unmanned Aerial Vehicle (UAV) in order to examine the best spectral response of red, blue, green, NIR bands and their combinations, as well as the best camera installation setup.

The purpose of the field campaign was to conduct tests on the potential practical applications of the image processing for river turbidity monitoring. This tool can promote the development of early warning networks at river basin scale, moving water research forward thanks to a large increase of data on water bodies and the reduction of operating expenses.

2.3 Full-scale experiment in Bode River case study

The field experiment took place in February 2023, in the monitoring station of Meisdorf, Germany, better described in Miglino et al. (2022). The selected river section was the Selke River, within the TERENO (TERrestrial ENvironmental Observatories) global change exploratory catchment managed by the Helmholtz Association, Germany (Wollschläger et al., 2017), showed in Figure 2.3.

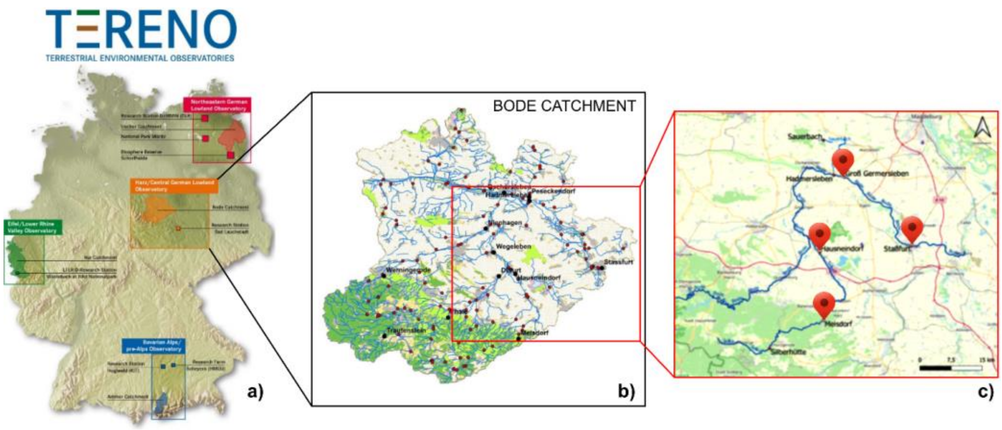

Figure 2.3: TERENO spans an Earth observation network (a) across Germany that extends from the North German lowlands to the Bavarian Alps, including the Bode catchment (b). The red markers (c) show the four most suitable UFZ monitoring stations within the Bode catchment for the on-site installation of the RGB camera.

Recently, the Bode basin has gone through prolonged droughts from 2015 to 2019, resulting in changes in land use, water quantity and quality (Zhou et al., 2022). This could potentially impact also the suspended solids load and pollutants concentration. In this experiment a synthetic turbidity event was recreated by adding kaolin clay into the water, upstream enough from the monitored river cross-section, to ensure the complete mixing of the tracer (Figure 2.4). Kaolin is usually exploited to prepare turbidity standard solutions. In addition, it is harmless, easy to handle, and a cheap mineral, which is also a common silicate in natural soils and sediments.

Figure 2.4: View of Selke River, before (a) and during (b) the synthetic turbidity peak in the field experiment.

We conducted the tracer experiment on 14 February 2023, adding 50 kg of kaolin tracer evenly distributed to the whole stream cross section at 12:05, 700 m upstream of the monitored river section. The mean flow velocity was 0.47 m/s, the flow discharge was 2.3 m^3/s, while the water level was 0.54 m, and the width of the river section was 9 m. The turbidity level started to artificially increase after 12:20, the peak was reached around 12:30, and the event ended after 13:00.

Several monitoring instruments were used during the experiment: three low-cost trap cameras (TC-Ceyomur CY50), one multispectral camera (MSC-Tetracam ADC Snap) and one unmanned aerial vehicle (UAV-DJI Mavic 2 Enterprise Dual) were placed in different positions. By looking at Figure 2.5, the MSC, in red, was installed on the bridge and the square in red represents its field of view. Two TCs were installed on the left riverbank (LRB) and the right riverbank (RRB), while the third TC was fixed on the bridge. The last camera was on the UAV, which ensured a zenithal field of view on the river section, indicated by the light blue square. The flight height of the UAV was 5 m. The data collected could be affected by sun-glint, shadows and other external light sources. For these reasons, it’s essential to find the optimum camera installation design, for minimizing the uncertainties from water images. The camera data was compared to the measurements of the turbidimeters installed underwater in the river cross-section (Figure 2.6). They were located with a distance of 2 m each from the right and left stream bank for ensuring to detect the complete mixing of the suspended solids. The artificial turbidity event generated a moderate-high turbidity level, peaking at 70 NTU.

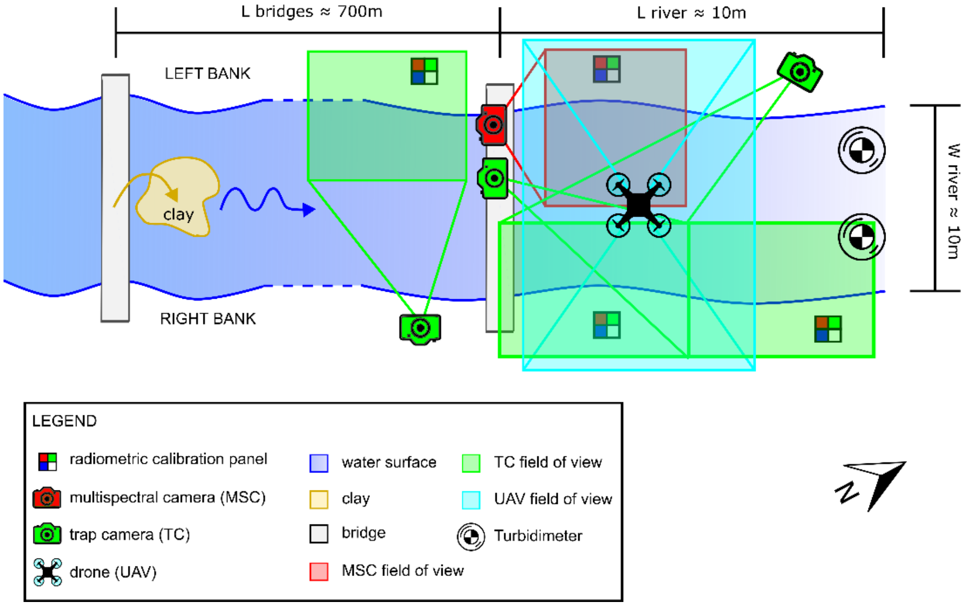

Figure 2.5: Plan of the monitored river section during the field experiment, showing the generated synthetic turbidity events, using kaolin clay tracer.

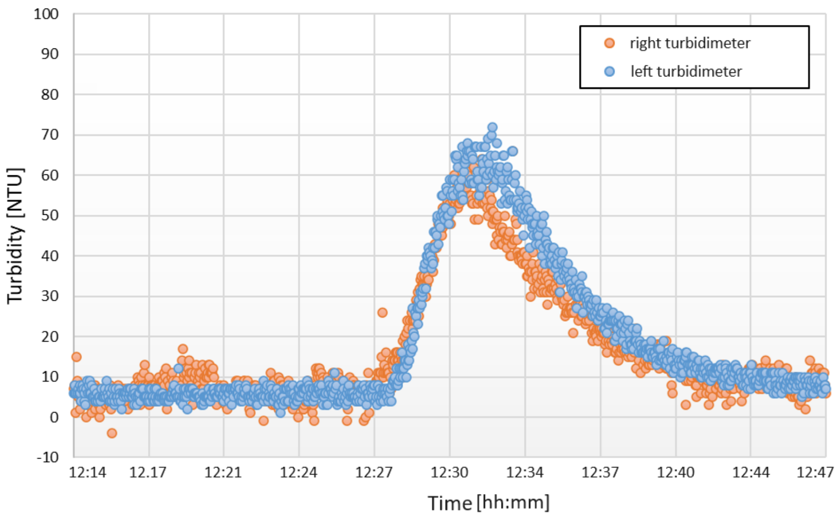

Figure 2.6: Optical measurements of turbidity, using two turbidimeters installed on the right and the left riverbed sides during the experiment.

The frame set in Figure 2.7 displays all the camera's fields of view along the stream during the experiment. The region of interest (ROI) was selected making sure that it included only the water surface area. The mean of the pixel values inside the ROI area was considered as the representative value for the turbidity level for each single picture. Moreover, a radiometric calibration panel (RCP) was installed within the picture area, close to the investigated water surface. It consisted of a waterproof plastic laminated panel containing the reference RGB color values for the image processing steps below.

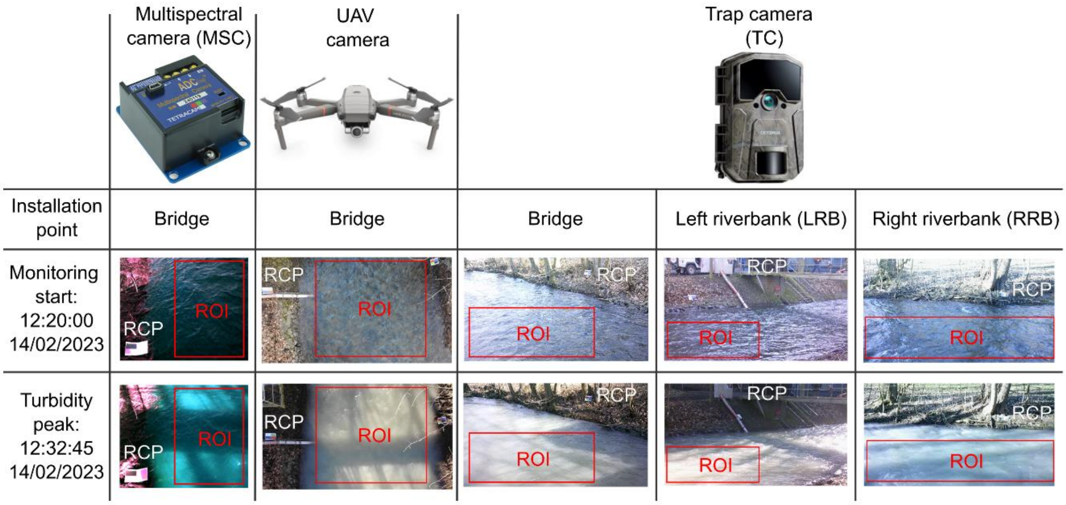

Figure 2.7: Frame set of the camera types, fields of view and installation points during the start and the peak event time of the field experiment.

The designed installation setup granted us the total or partial superimposition of the view fields of the different cameras, in order to analyze approximately the same water surface area.

2.4 Image processing procedure

This work defines and tests an image-based method that takes into account variables occurring within time- and site-specific riverine environments. It's important to build a robust procedure, since the acquired camera data cannot provide information as they are because they are not yet compared to physically meaningful units. Herein, our workflow (Figure 2.8) sets out the general algorithm of image processing for turbidity analysis, starting from a correct image extraction and stabilization. Then, the steps of radiometric calibration and binarization allowed us to homogenize and select the relevant features from the image data. Finally, the indexes were defined from processed signals and validated by field measurements to train the model and quantify the river turbidity level.

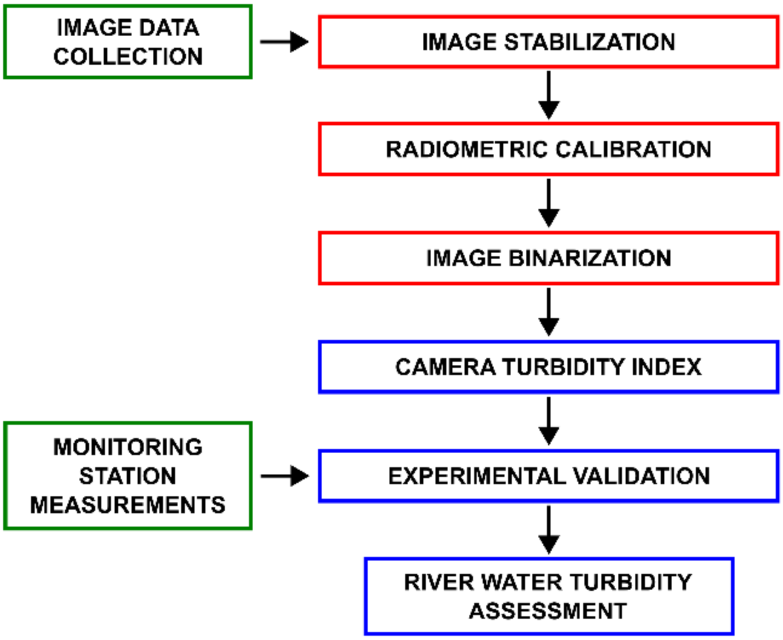

Figure 2.8: Image processing procedure workflow.

2.4.1 Image extraction and stabilization

The image data were stored as timelapses with a set frame rate depending on the type of camera. The number and the format of the extracted images were fixed for each timelapse frame, also annotating frequencies, to ensure the correct comparison between cameras and measurement data.

The image sequences were involved in the image stabilization process, because the position of the objects in the scene could be shifted by environmental factors and camera instability. The image stabilization techniques performed an automatic detection and matching of features within the selected image area close to the RCP (Figure 2.9). In particular, we used the Harris-Stephens corner detection algorithm to identify feature points and remove apparent movements and jitter within the field of view in the videos (Harris & Stephens, 1988; Abdullah et al., 2012). This step was necessary to grant the correct detection of the RCP and ROI areas location required for the following image analysis processes.

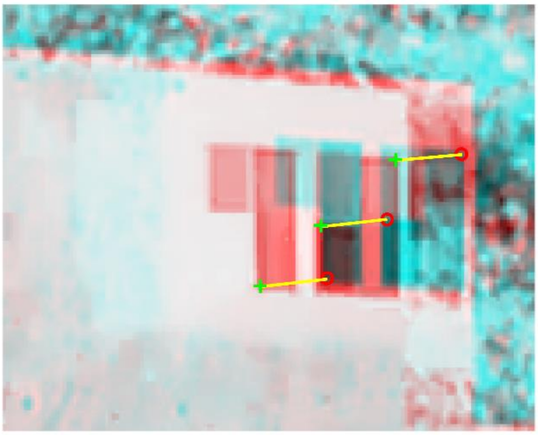

Figure 2.9: Stabilization of the RCP coordinates for each extracted frame. The yellow lines show the panels shift during a camera monitoring period of two months.

2.4.2 Radiometric calibration

For absolute radiometric correction in monitoring activities where the distance between the ground and the camera is less than 100 meters, it is assumed that the atmosphere is not influencing the light signal. Nevertheless, other site-specific and meteorological variables can still affect the camera measurement (Daniels et al., 2023). The radiometric signal of an object is influenced by the geometry of the measurements, depending on the relative positions of the sun, the measured object and the optical sensor. The direct-diffuse ratio, the atmosphere absorption, and scattering of the solar radiation in the space from the object to the sensor, and also the camera sensitivity are all significant factors affecting the detection of the natural illumination conditions. Using reference targets or recognized radiometric standards within the scene is necessary to convert the uncalibrated image pixel intensity (PI) values, also called digital numbers (DNs), into radiometrically meaningful units such as reflectance or radiance (Guo et al., 2019; Kinch et al., 2020). In this experiment, we chose a simplified design of the radiometric calibration panel with inside the assumed reference values (RV_{rc}) of the maximum PIs of red, green and blue for all the image (Figure 2.10b), considered as the mean of the respective single band values of the pixels inside the panel squares.

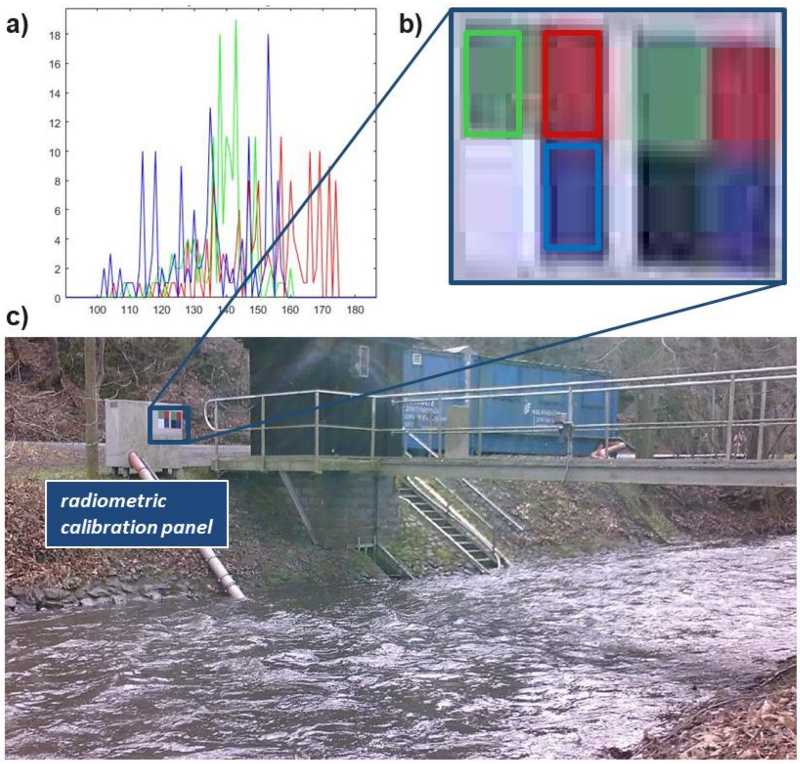

Figure 2.10: Example of radiometric calibration procedure applied to a TC image, using the reference mean RGB values (a) of the radiometric calibration panel (b) installed within the camera field of view (c).

The image PI values were reassigned considering the RCP reference values frame by frame, for each band, as follow:

$$PIrc = \{ 1 , PI/RV_{rc}\}, \quad (1)$$

where RV_{rc} is the panel reference value of red, green and blue for the radiometric calibration process.

PI values range for each band can go from 0 to 255, but we considered normalized values between 0 and 1. Once the radiometric signal is correctly calibrated, the effect of changes in light conditions on the image information is substantially reduced. Therefore, some image areas could still be affected by sun glare and overly intense shadow. These pixels must be removed by binarization because they do not contain useful information about the water reflectance.

2.4.3 Binary masking

Image binarization techniques convert images into binary representations typically applying predetermined thresholds to grayscale or RGB values. Here, the adopted procedure follows the Otsu's approach (Otsu, 1975). The global threshold was defined, separately for each band and for each frame, as a result of the minimization of the weighted variance of two clusters. All the values above this threshold are replaced with 1, while the other values with 0. The procedure involves iterations through every image pixel and counts the occurrence of each intensity. In this way, only the actual water reflectance information can be retrieved from the pictures.

More in detail, looking at Figure 2.11, we obtained a perfect binary masking from the starting RGB image. Thanks to the right combination of the binarized bands, we managed to remove the pixels with signal distortions due to the effect of sun glare, shadows and also external objects such as the branches that fall inside the camera RoI, bordered by the red line in the figure. Moreover, this step of the procedure highlights the importance of the information contained in each band. For example, the blue band is not effective in turbidity estimation, but it allows us to isolate and remove critical parts of the image

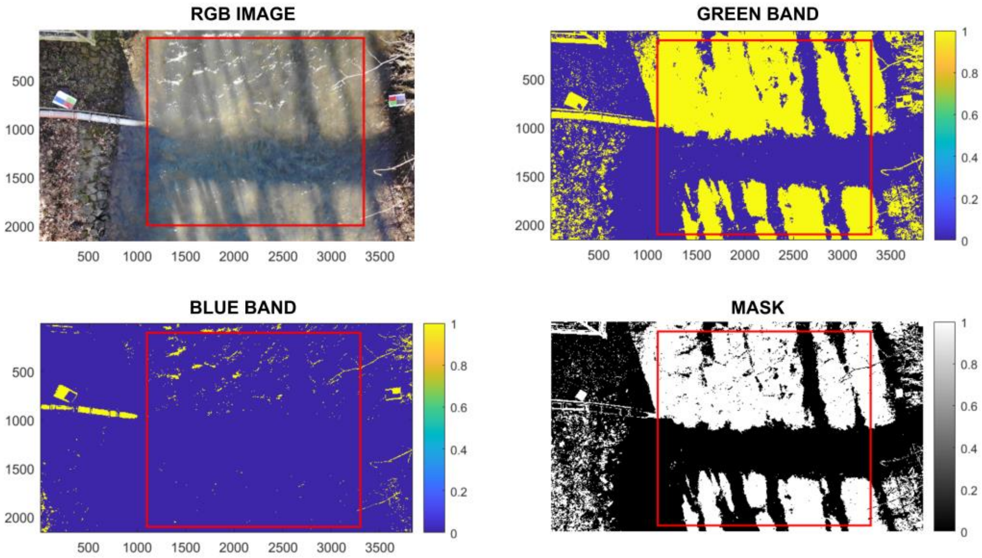

Figure 2.11: UAV image masking with binarization procedure

2.4.4 Camera index of river turbidity

There are several applications of river turbidity monitoring from satellites which provide a clear overview of the opportunities offered by different spectral indices (e.g. Fraser,1998; Lacaux et al., 2007; Wang and Shi, 2007; Constantin et al., 2016). Among others, Garg et al. (2020) investigated the change in spectral reflectance of water across the visible to near-infrared (NIR) range along the Ganga River. The temporal analysis indicates a reduction in reflectance across the visible-to-NIR range, likely due to decreased water turbidity. While it is difficult to use the blue and green bands to map variations because of bottom interference, the red and NIR bands prove more sensitive for turbidity estimation, particularly in optically deep water. The study of Hossain et. al. (2021) seems to confirm it. They obtained good results with Landsat observations of the Tennessee River in USA, finding a relationship between turbidity and the red band reflectance. The results of Lobo et al. (2015) confirm the strong relationship between red band and total suspended solids in the case study of Tapajos River in Amazon, also using Landsat data. Ehmann et al. (2019) supported their arguments, emphasizing the red band's sensitivity in detecting changes in turbidity level within in a small river using UAS imagery.

In our study we considered all the available camera bands for getting information on the monitored river site. We selected the most representative remote sensing applications for each band and index, as explained in Table 2.1.

Band Combination		Camera	Reference
Red / Green		TC, MSC, UAV	Wang et al.,(2006)
NDTI		TC, MSC, UAV	Lacaux et al.,(2007)
NDWI		MSC	McFeeters,(1996)
Single Bands	Red	TC, MSC, UAV	Leeuw & Boss,(2018)
	Green	TC, MSC, UAV	Khorram et al.,(1991)
	NIR	MSC	Zhu et al.,(2020)

Table 2.1: Camera band combinations selected for on-site river turbidity remote measurements

Single green and red bands were considered the most representative signals for identifying the turbidity. The NIR band is also effective in detecting very high turbidity levels. Some ratios between these bands were taken into account too. We selected from literature the ratio between red and green, the normalized difference turbidity index (NDTI) derived from RGB-imagery and the normalized difference water index (NDWI) that combine NIR and green bands.

2.5 Experimental results

This section is going to show and explain the results obtained with the field campaign of February 2023 in Bode basin. All the results are considered as already processed (see Section 2.4), unless otherwise specified in the description.

The experiment highlighted the capability of digital cameras to detect variations in turbidity level. We observed that digital camera results are influenced by several factors, such as the type of sensor adopted, the camera sensitivity, position and orientation. In particular, MSC results in Figure 2.12 describe distinct behaviours of the single bands. Red and green bands can capture increases above the measured value of 20 NTU, while the NIR band spectral response is much lower. Since the NIR band is totally absorbed by the water surface, its substantial changes can be detected only for very high concentrations of suspended particles. If we consider the NDWI, the correlation between the camera and turbidimeter data becomes more consistent, as well as those of red and green bands.

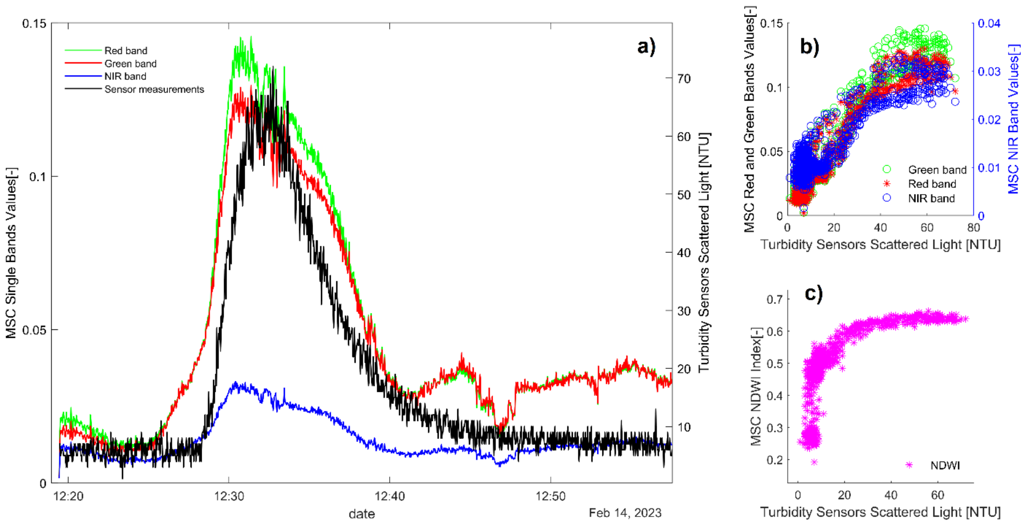

Figure 2.12: a) Comparison between turbidimeter measurements and data from the multispectral camera (MSC) installed on the bridge; b) Scatter plot of the MSC single bands values and on-site measurements; c) Scatter plot of the MSC NDWI values and on-site measurements.

Trap camera outcomes are reported in Figure 2.13, where it is possible to observe different patterns depending on the installation position. Red and green band signals, from the TCs installed on the LRB and RRB, follow the measurement curve for the entire monitoring period, while the TC installed on the bridge seems to be influenced by the variation of the light condition during the first part of the experiment, before exceeding values higher than 50 NTU. Moreover, all the TCs results show the same intensity values in correspondence to the turbidity peak, except those from LRB matching the measures but with lower PI signals. The most reliable TC bands ratios and indexes were those from the RRB position (Table 2).

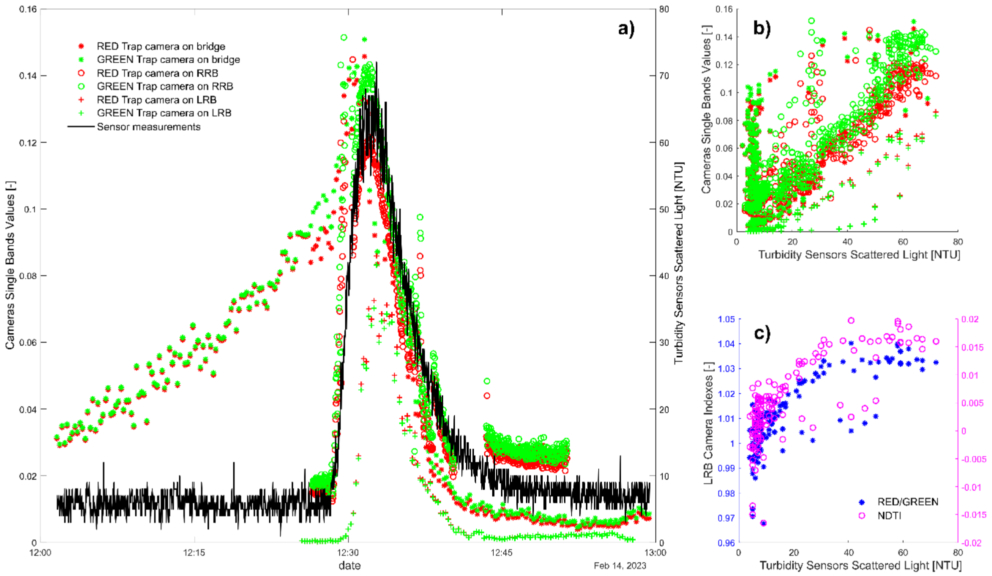

Figure 2.13: Comparison between turbidimeter measurements, red and green band values from all the trap cameras installed on site; b) Scatter plot of all the cameras green band signal (in green) and red band signal (in red); c) Scatter plot of the NDTI (in magenta) and Red/Green (in blue) indexes from the trap camera installed on the left riverbank (LRB).

The UAV camera returned partial data (Figure 2.14), due to the loss of signal that caused a break in the recordings for 5 minutes immediately after reaching the measured turbidity peak. Therefore, there is a good correspondence between UAV bands signal and the turbidimeter data. In the second part of the recording, we can observe that the bands signals are lower than those during the peak, but they don't exactly fit the measurements decreasing curve. That's because the white balance setting of the camera was on and this resulted in a discrepancy in the intensity of the starting signals, but not in terms of variations.

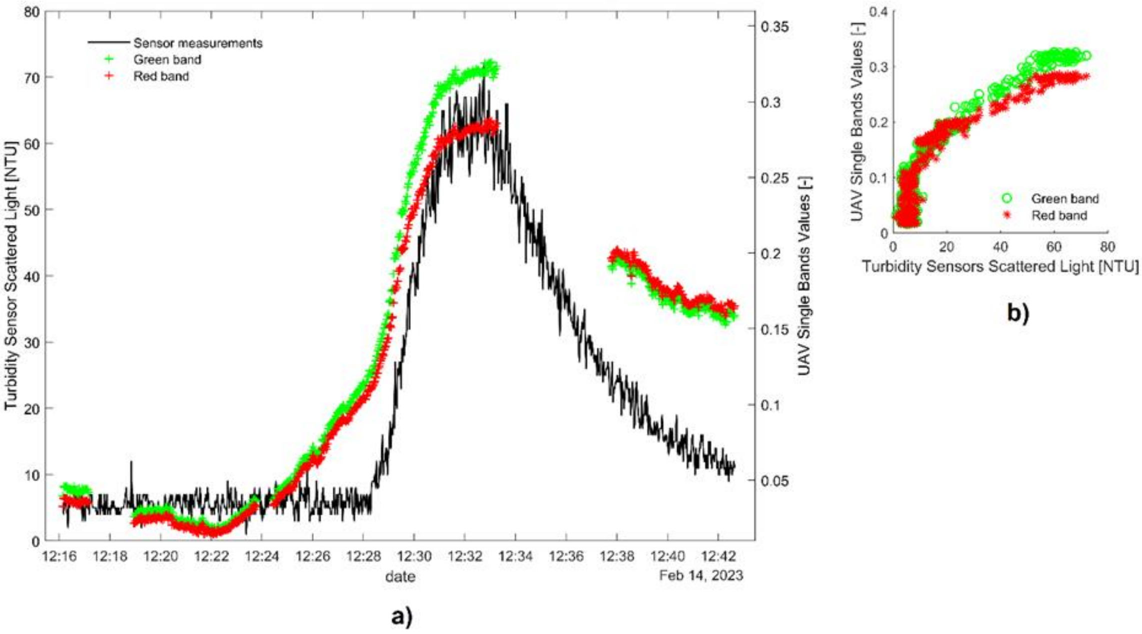

Figure 2.14: a) Comparison between turbidimeter measurements and data from the UAV camera; b) Scatter plot of the variables.

On one hand, the zenithal angle of UAV camera ensured us a clear and wide view on the entire river section and a good sensitivity to turbidity variations.

On the other hand, the UAV battery life, less than one hour, is a strong limitation for long terms monitoring activities, even for a few hours experiment like this.

This is one of the reasons why we have decided to focus only on fixed cameras in the second experiment of June 2023, explained in detail within the following Section 3.

Furthermore, the performance metrics of these experimental results are discussed in Section 4.

2.6 References

Abdullah, L. M., Tahir, N. M., & Samad, M.: Video stabilization based on point feature matching technique, 2012 IEEE Control and System Graduate Research Colloquium, pp. 303-307, IEEE, 10.1109/ICSGRC.2012.6287181, 2012.

Constantin, S., Doxaran, D., & Constantinescu, Ș.: Estimation of water turbidity and analysis of its spatio-temporal variability in the Danube River plume (Black Sea) using MODIS satellite data, Continental shelf research, 112, 14-30, https://doi.org/10.1016/j.csr.2015.11.009, 2016.

Daniels, L., Eeckhout, E., Wieme, J., Dejaegher, Y., Audenaert, K., & Maes, W. H.: Identifying the Optimal Radiometric Calibration Method for UAV-Based Multispectral Imaging, Remote Sensing, 15(11), 2909, https://doi.org/10.3390/rs15112909, 2023.

Droujko, J., & Molnar, P. (2022). Open-source, low-cost, in-situ turbidity sensor for river network monitoring, Scientific Reports, 12(1), 10341.

Ehmann, K., Kelleher, C. and Condon, L.E., Monitoring turbidity from above: Deploying small unoccupied aerial vehicles to image in-stream turbidity. Hydrological Processes, 33(6), pp.1013-1021, 2019.

Fraser, R.N., 1998. Multispectral remote sensing of turbidity among Nebraska Sand Hills lakes. International Journal of Remote Sensing, 19(15), pp.3011-3016.

Garg, V., Aggarwal, S. P., & Chauhan, P.: Changes in turbidity along Ganga River using Sentinel-2 satellite data during lockdown associated with COVID-19, Geomatics, Natural Hazards and Risk, 11(1), 1175-1195, https://doi.org/10.1080/19475705.2020.1782482, 2020.

Gholizadeh, M. H., Melesse, A. M., & Reddi, L.: A comprehensive review on water quality parameters estimation using remote sensing techniques, Sensors, 16(8), 1298, https://doi.org/10.3390/s16081298, 2016.

Ghorbani, M. A., Khatibi, R., Singh, V. P., Kahya, E., Ruskeepää, H., Saggi, M. K., ... & Jani, R.: Continuous monitoring of suspended sediment concentrations using image analytics and deriving inherent correlations by machine learning, Scientific reports, 10(1), 8589, https://doi.org/10.1038/s41598-020-64707-9, 2020.

Goddijn-Murphy, L., Dailloux, D., White, M., & Bowers, D.: Fundamentals of in situ digital camera methodology for water quality monitoring of coast and ocean, Sensors, 9(7), 5825-5843, https://doi.org/10.3390/s90705825, 2009.

Goddijn, L. M., & White, M.: Using a digital camera for water quality measurements in Galway Bay. Estuarine, coastal and shelf science, 66(3-4), 429-436, https://doi.org/10.1016/j.ecss.2005.10.002, 2006.

Guo, Y., Senthilnath, J., Wu, W., Zhang, X., Zeng, Z., & Huang, H.: Radiometric calibration for multispectral camera of different imaging conditions mounted on a UAV platform, Sustainability, 11(4), 978, https://doi.org/10.3390/su11040978, 2019.

Harris, C., & Stephens, M.: A combined corner and edge detector, Alvey vision conference (Vol. 15, No. 50, pp. 10-5244, 1988.

Hossain, A. A., Mathias, C., & Blanton, R.: Remote sensing of turbidity in the Tennessee River using Landsat 8 satellite, Remote Sensing, 13(18), 3785, https://doi.org/10.3390/rs13183785, 2021.

Jia, K., Hasan, U., Jiang, H., Qin, B., Chen, S., Li, D., ... & Shen, J.: How frequent the Landsat 8/9-Sentinel 2A/B virtual constellation observed the earth for continuous time series monitoring, International Journal of Applied Earth Observation and Geoinformation, 130, 103899, https://doi.org/10.1016/j.jag.2024.103899, 2024.

Khorram, S., Cheshire, H., Geraci, A. L., & ROSA, G. L.: Water quality mapping of Augusta Bay, Italy from Landsat-TM data. International Journal of Remote Sensing, 12(4), 803-808, https://doi.org/10.1080/01431169108929696, 1991.

Kinch, K. M., Madsen, M. B., Bell, J. F., Maki, J. N., Bailey, Z. J., Hayes, A. G., ... & Winhold, A.: Radiometric calibration targets for the Mastcam-Z camera on the Mars 2020 rover mission, Space science reviews, 216, 1-51, https://doi.org/10.1007/s11214-020-00774-8, 2020.

Lacaux, J. P., Tourre, Y. M., Vignolles, C., Ndione, J. A., & Lafaye, M.: Classification of ponds from high-spatial resolution remote sensing: Application to Rift Valley Fever epidemics in Senegal, Remote sensing of environment, 106(1), 66-74, https://doi.org/10.1016/j.rse.2006.07.012, 2007.

Leeuw, T., & Boss, E.: The HydroColor app: Above water measurements of remote sensing reflectance and turbidity using a smartphone camera. Sensors, 18(1), 256, https://doi.org/10.3390/s18010256, 2018.

Lobo, F. L., Costa, M. P., & Novo, E. M.: Time-series analysis of Landsat-MSS/TM/OLI images over Amazonian waters impacted by gold mining activities. *Remote Sensing of Environment*, *157*, 170-184, 2015.

Lu, Y., Chen, J., Xu, Q., Han, Z., Peart, M., Ng, C. N., ... & Law, W. W.: Spatiotemporal variations of river water turbidity in responding to rainstorm-streamflow processes and farming activities in a mountainous catchment, Lai Chi Wo, Hong Kong, China. Science of The Total Environment, 863, 160759, https://doi.org/10.1016/j.scitotenv.2022.160759, 2023.

Luo, Y., Doxaran, D., Ruddick, K., Shen, F., Gentili, B., Yan, L., & Huang, H., Saturation of water reflectance in extremely turbid media based on field measurements, satellite data and bio-optical modelling. Optics express, 26(8), 10435-10451, 2018.

Manfreda, S., Ben Dor, E.: Unmanned Aerial Systems for Monitoring Soil, Vegetation, and Riverine Environments, Earth Observation Series, Elsevier, ISBN: 9780323852838, 2023.

Manfreda S, McCabe MF, Miller PE, Lucas R, Pajuelo Madrigal V, Mallinis G, Ben Dor E, Helman D, Estes L, Ciraolo G, et al. On the Use of Unmanned Aerial Systems for Environmental Monitoring, Remote Sensing, 10(4):641, https://doi.org/10.3390/rs10040641, 2018.

McFeeters, S. K.: The use of the Normalized Difference Water Index (NDWI) in the delineation of open water features. International journal of remote sensing, 17(7), 1425-1432, https://doi.org/10.1080/01431169608948714, 1996.

Miglino, D., Jomaa, S., Rode, M., Isgro, F., & Manfreda, S.: Monitoring Water Turbidity Using Remote Sensing Techniques. Environmental Sciences Proceedings, 21(1), 63, https://doi.org/10.3390/environsciproc2022021063, 2022.

Nechad, B., Ruddick, K. G., & Park, Y.: Calibration and validation of a generic multisensor algorithm for mapping of total suspended matter in turbid waters, Remote Sensing of Environment, 114(4), 854-866, https://doi.org/10.1016/j.rse.2009.11.022, 2010.

Potes, M., Costa, M. J., and Salgado, R.: Satellite remote sensing of water turbidity in Alqueva reservoir and implications on lake modelling, Hydrol. Earth Syst. Sci., 16, 1623–1633, https://doi.org/10.5194/hess-16-1623-2012, 2012.

Otsu, N.: A threshold selection method from gray-level histograms. Automatica, 11(285-296), 23-27, 1975.

Wang, F., Han, L., Kung, H. T., & Van Arsdale, R. B.: Applications of Landsat-5 TM imagery in assessing and mapping water quality in Reelfoot Lake, Tennessee, International Journal of Remote Sensing, 27(23), 5269-5283, https://doi.org/10.1080/01431160500191704, 2006.

Wang, M. and Shi, W., 2007. The NIR-SWIR combined atmospheric correction approach for MODIS ocean color data processing. Optics express, 15(24), pp.15722-15733.

Wollschläger, U., Attinger, S., Borchardt, D., Brauns, M., Cuntz, M., Dietrich, P., ... & Zacharias, S.: The Bode hydrological observatory: a platform for integrated, interdisciplinary hydro-ecological research within the TERENO Harz/Central German Lowland Observatory. Environmental Earth Sciences, 76, 1-25, https://doi.org/10.1007/s12665-016-6327-5, 2017.

Zhou, X., Jomaa, S., Yang, X., Merz, R., Wang, Y., & Rode, M.: Exploring the relations between sequential droughts and stream nitrogen dynamics in central Germany through catchment-scale mechanistic modelling. *Journal of Hydrology*, *614*, 128615, 2022.

Zhu, Y., Cao, P., Liu, S., Zheng, Y., & Huang, C.: Development of a new method for turbidity measurement using two NIR digital cameras, Acs Omega, 5(10), 5421-5428, https://doi.org/10.1021/acsomega.9b04488, 2020.

3 Application of the procedure in changing hydrological conditions

Herein, the proposed image processing procedure has been tested in a second experiment of June 2023, for estimating the turbidity level in the same river section with a similar camera's installation setup, but this time using three different tracers, varying in colour and concentration of the suspended particles. The observed environmental and hydrological conditions was drastically different respect to the previous experiment in terms of vegetation cover, lights and shadows direction and intensity, water level and flow velocity. These conditions were necessary to stress the procedure as much as possible, in order to generalize it and to deepen its potential for real river monitoring applications.

In Section 3, the artificial water turbidity perturbation and the camera's installation setup of the second experiment are explained in detail. To follow, the best performing bands and range of applicability of the procedure are shown. Lastly, the results of both experiments are compared to evaluate the reliability of the procedure for long term monitoring.

3.1 Second experiment in Bode River

The second field experiment took place in June 2023, in the monitoring station of Meisdorf, Germany, already described in Section 2.

In this experiment the synthetic turbidity event was split in three phases, as shown in Figure 3.2. The event was recreated by adding different tracers, in this order: kaolin clay, dolomite flour and lava flour. The three tracers were added into the water upstream enough from the monitored river cross-section, to ensure the complete mixing of the suspended particles (Figure 3.1). During the experiment, the mean flow velocity was 0.29 m/sec, the flow discharge was 0.4 m3/s, while the water level was 0.21 m, and the width of the river section was 6.5 m.

First, we added 25 kg of kaolin tracer evenly distributed to the whole stream cross section at 10:50, 700 m upstream of the monitored river section. The turbidity level started to artificially increase after 11:20, the peak was reached around 11:30, and the event ended after midday.

Then, we added another 25 kg of dolomite flour tracer from the same spot at 11:50, to avoid the overlapping of the two consecutive events. The turbidity level started to increase after 12:20, the peak was reached around 12:30, and the event ended after 12:55.

Lastly, we added 25 kg of lava flour tracer from a closer river section, 250 m upstream of the monitored section, at 12:50. This time, the turbidity increased after 13:00 and the peak was reached very quickly around 13:04, and the event ended almost equally fast after 13:10, reaching a considerably higher peak due to the closer input spot of the tracer.

The monitoring instruments used were one low-cost trap cameras (TC-Ceyomur CY50), one multispectral camera (MSC-Tetracam ADC Snap) and one more expensive digital camera (DC-Nikon Coolpix P950) fixed in different positions. By looking at Figure 3.1, the MSC, in red, the TC and the DC, were installed on the bridge and the squares, respectively in red, light blue and green, represent their fields of view.

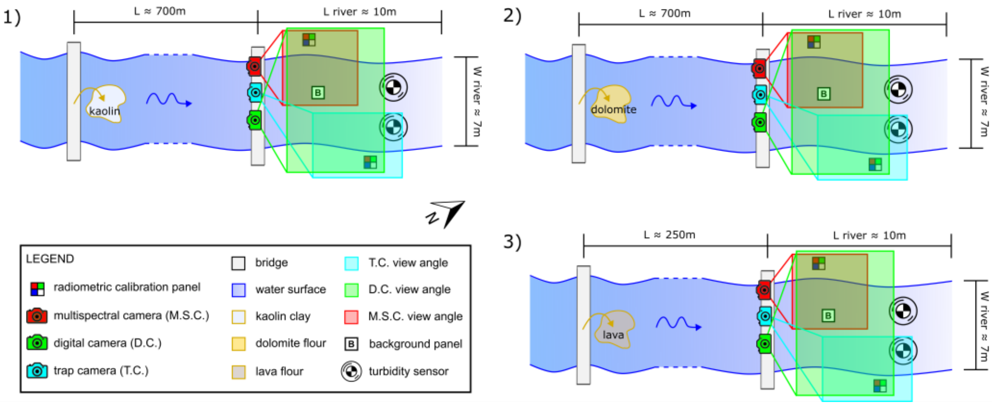

Figure 3.1: Plan of the monitored river section during the field experiment, showing the generated synthetic turbidity events, using kaolin clay (1), dolomite (2) and lava (3) tracers.

Unlike the first, this experiment focused more on the camera's capability of recognizing variations in turbidity due to suspended particles changing in optical properties and concentrations, rather than the installation setups of the sensors.

The camera data were compared to the measurements of the turbidimeters (Figure 3.2) installed underwater in the river cross-section. They were located with a distance of 2 m each from the right and left stream bank for ensuring to detect the complete mixing of the suspended solids. The artificial events generated moderate and very high turbidity levels, peaking at 180 NTU.

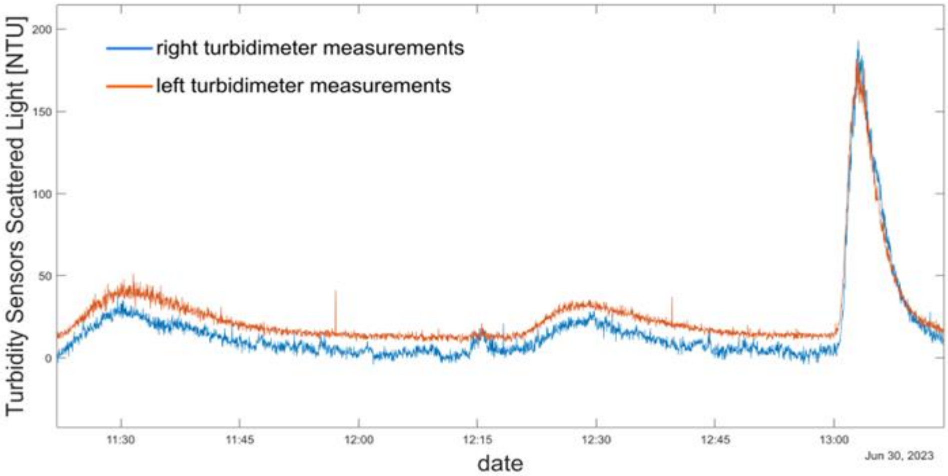

Figure 3.2: Optical measurements of turbidity, using two turbidimeters installed on the right and the left riverbed sides during the experiment.

3.2 Effect of the riverbed background on the procedure

The frame set in Figure 3.3 displays all the camera's view fields of the Selke stream during the experiment. The region of interest (ROI) was selected making sure that it included only the water surface area. The mean of the pixel values inside the ROI area was considered as the representative value for the turbidity level for each single picture.

A first radiometric calibration panel (RCP), designed in the same way of the first experiment, was installed within the image area, close to the investigated water surface. This time, we decided to add a second RCP fixed on the riverbed, since the water level was quite shallow and the riverbed component of the total reflectance reaching the camera lenses was substantial, especially for low turbidity level, as explained in Section 2.1.

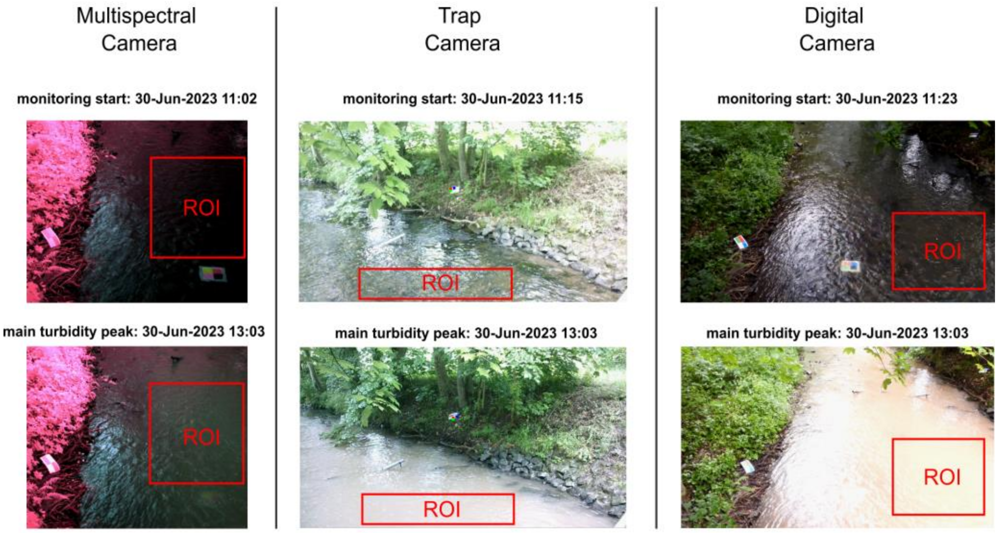

Figure 3.3: Frame set of the camera types, fields of view and installation points during the start and the peak event time of the field experiment.

The use of a submerged RCP panel helped us in removing the effect of BG reflectance during the experimental monitoring. By looking at MSC and DC images in Figure 3.4, where the submerged RCP is within their fields of view, the water was clear (NTU<20), and the panel was visible before the artificial increase of the turbidity level. As shown by the results in the next section, our cameras detected high PI values within the ROI also for the initial condition of clear water (CW), and then recorded an increase of PIs during the turbidity event recreated.

Therefore, variable flow and light conditions within the monitored river section could generate different spectral responses of the water, even if the river turbidity level is the same. This issue is evident in Section 3.4 where the results of both the experiments show different initial PI signals for the same starting CW conditions, due to the change in hydrological and environmental conditions between the experiment of February and the experiment of June.

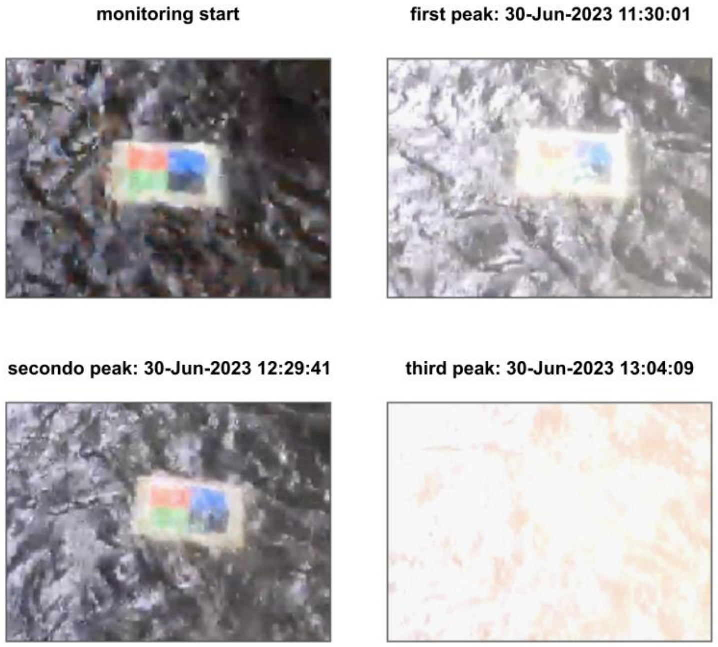

Figure 3.4: Frame set of the submerged RCP during the monitoring start and the three peaks of the turbidity event artificially recreated within the field experiment.

For these reasons, we decided to use the PI value of the submerged RCP as reference. During the two experiments, it was noted that the increments of PI values were comparable to the actual turbidity level increases, although the gap in the starting PI values during the CW conditions.

The assumptions are explained in detail in Section 3.3.1.

3.3 Sensitivity analysis of the experimental results

The section below is going to show and explain the experimental results obtained with the second field campaign of June 2023 in Bode basin. All the results are considered as already processed (see Section 2.4), unless otherwise specified in the description.

In Figure 3.5A, the unfiltered red band data from digital camera follows the behavior of turbidity level for the three synthetic events, although overestimating the first two peaks, due to changes in light conditions during the first part of the experiment.

In Figure 3.5B, the process of image binarization minimizes the effect of sun glint within the ROI excluding the saturated pixels.

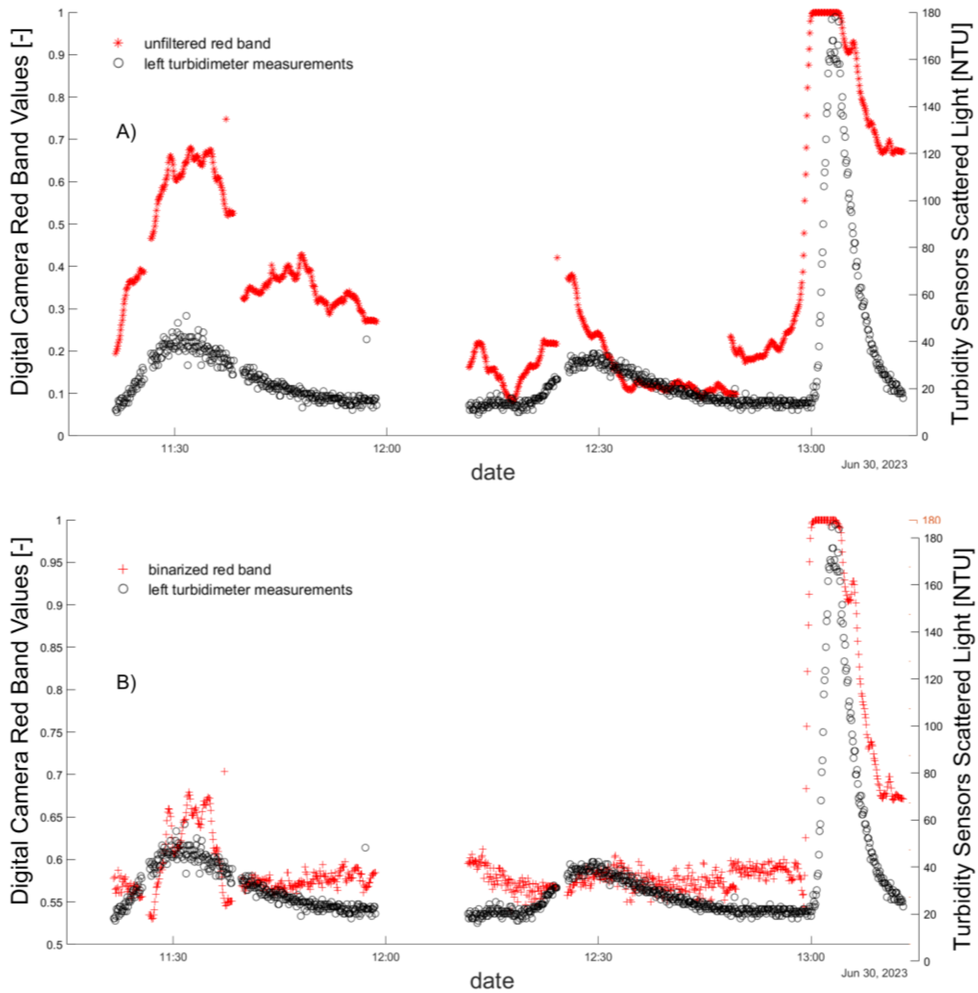

Figure 3.5: Comparison of turbidity measurements with unfiltered (A) and binarized (B) digital camera red band data.

In contrast to graph 3.5A, the data points in graph 3.5B are more closely aligned, indicating a stronger correlation between the image data and measurements. This confirms that the use of image processing procedure enhances the predictions of the digital camera. However, the matching is still not perfect, in particular for the second turbidity event, the lowest, highlighting the importance of a rigorous calibration and elaboration of the images, to ensure consistent results in changing environmental conditions.

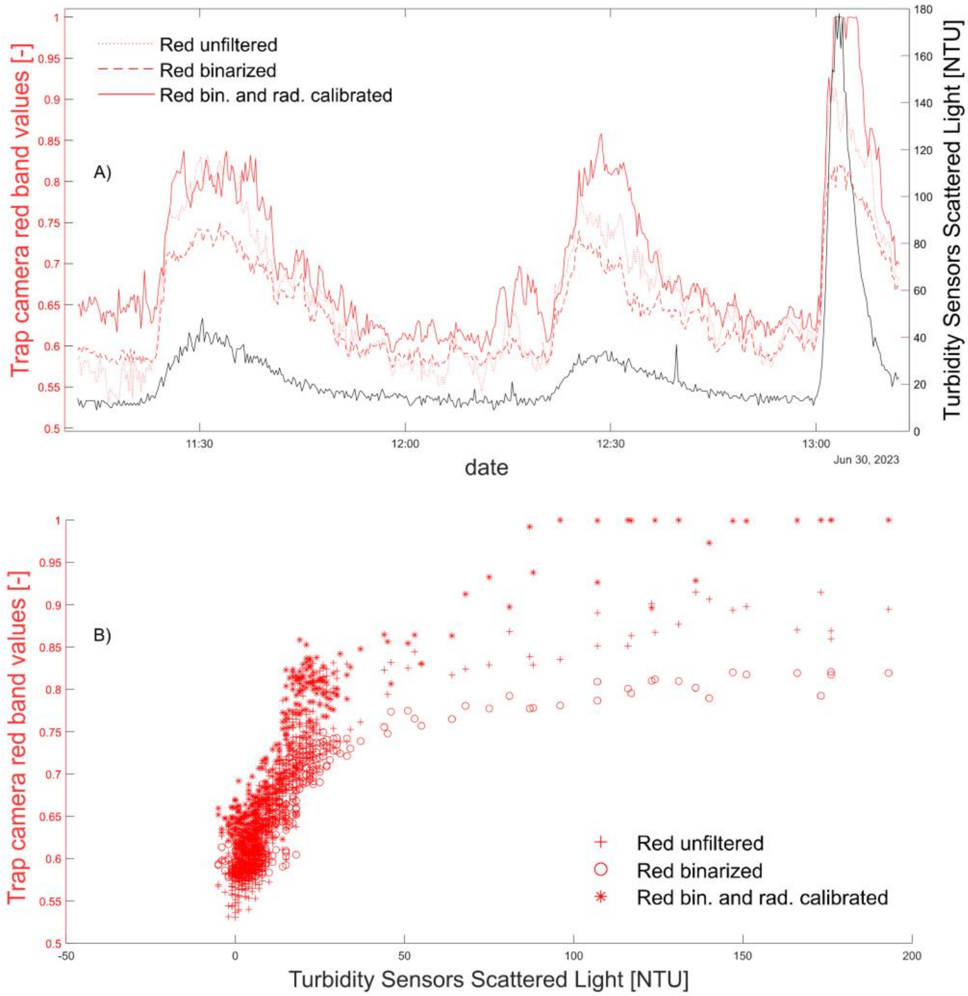

Figure 3.6: A) Comparison between turbidimeter measurements (in black) and TC red band behaviour during the synthetic turbidity events of June 2023, considering the camera data unfiltered (dotted red line), the binarized (dashed red line), and binarized and radiometric calibrated (red line); B) Scatter plot of the variables.

Trap camera results are shown in Figure 3.6, for the single red band and the different image processing steps. The TC data was able to describe turbidity variations for all the three events. The image filtering provided a wider range of correlations between measurements and PI values.

The NDTI behaviour for TC data (Figure 3.7) describes a clear correspondence with measurements only for the higher turbidity values during the third peak. The process of the images provided also an increment of camera data during the first two peaks, but often presenting excessive divergence between the variables for lower turbidity values.

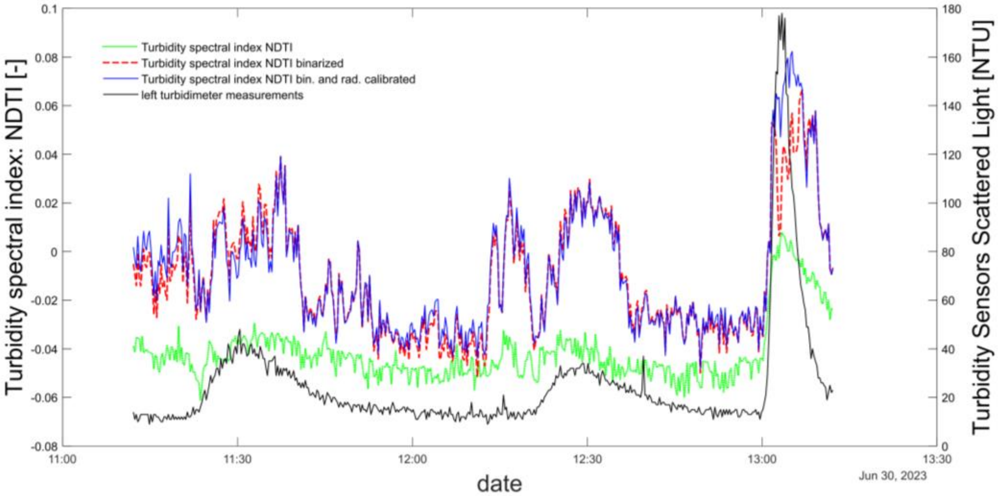

Figure 3.7: Comparison between turbidimeter measurements (in black) and TC NDTI index behaviour during the synthetic turbidity events of June 2023, considering the camera data unfiltered (green line), the binarized (dashed red line), and binarized and radiometric calibrated (blue line)

It was not possible to investigate the effect of BG reflectance for the trap camera results, because the TC view field didn't include the BG radiometric panel, as shown in Figure 3.3.

3.3.1 Use of riverbed background for turbidity estimation

The addition of the BG panel, namely the radiometric calibration panel on the riverbed, allowed us to measure also the PI values within the BG panel, in particular the pixel intensity of its black pane.

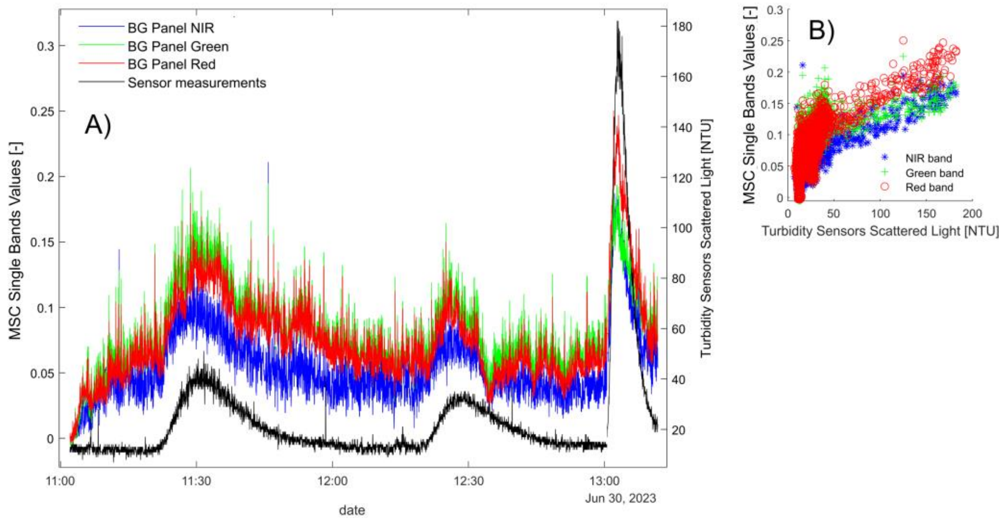

Figure 3.8: Comparison between turbidimeter measurements and the MSC bands PI values of the black pane within the submerged BG panel; B) Scatter plot of the variables

We can observe in Figure 3.8A that the starting PI values of the MSC bands for the black pane of BG panel were close to 0, because the turbidity level was very low. When the water was clear, the BG panel was completely visible and the black pane absorbed most of the light. In this condition, the riverbed reflectance affected the camera monitoring too much. Nevertheless, during the three turbidity events, there were sudden increases and decreases of the black pane PIs, because the BG panel was no longer plainly visible and the component of the water reflectance became bigger than the riverbed reflectance. For this reason, we assumed the non-visibility condition of the BG panel as the lower bound for camera monitoring.

Then, we defined a specific threshold for each MSC band, where the PI values within the ROI of river surface were measured only for the non-visibility condition of the BG panel's black pane. While, under these thresholds, the PI values was considered equal to the BG black pane PI for the clear water condition.

Figure 3.9 illustrates the behavior of the turbidity measurements alongside data from the red, green, and near-infrared (NIR) bands from the multispectral camera (MSC) filtered using the submerged BG panel, as explained above.

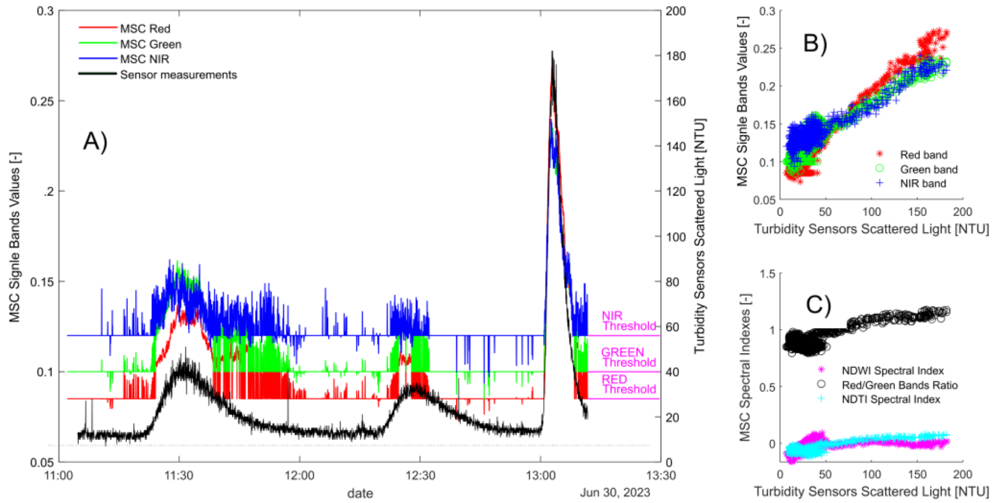

Figure 3.9: A) Comparison between turbidimeter measurements and MSC red, green and NIR bands data for the three synthetic turbidity events of June 2023; B) Scatter plot of the variables, considering single bands and measurements; C) Scatter plot of the variables, considering NDTI, NDWI, Red/Green index and measurements.

In detail, Figure 3.9A presents a time series comparison of the variables. A strong correlation is observed between the sensor measurements (black line) and the red, green, and NIR band values during the three peaks of the synthetic event, with high levels of turbidity. The NIR band (blue line), however, shows a more subdued response, remaining above its defined threshold for most of the monitored experiment. The scatter plot in Figure 3.9B confirms that NIR band reflectance starts to be detected by the camera lens for higher NTU than other RGB wavelengths.

While, Figure 3.9C shows the relationship between various spectral indices and the turbidity sensor measurements. Three indices are analyzed: NDWI (black circles), Red/Green band ratio (magenta circles), and NDTI (cyan circles). The Red/Green ratio shows a distinct increase with higher turbidity levels, suggesting that it is a reliable indicator for turbidity detection. Meanwhile, the NDWI and NDTI indices display more stable trends, with the NDWI being less sensitive to the variations in turbidity as the scattered data points maintain a nearly constant range regardless of NTU values. This indicates that while the Red/Green ratio effectively captures turbidity changes, the other two indices may require further investigation to enhance their sensitivity to high sediment concentrations.

Overall, the figure demonstrates that the MSC red and green bands, also through the Red/Green bands ratio and NDTI index, are well-suited for monitoring turbidity changes, with a strong alignment to turbidimeters readings starting from a moderately turbid water (NTU>30). The NIR band's response suggests its utility might be constrained to specific applications, offering a good match with high turbidity measures.

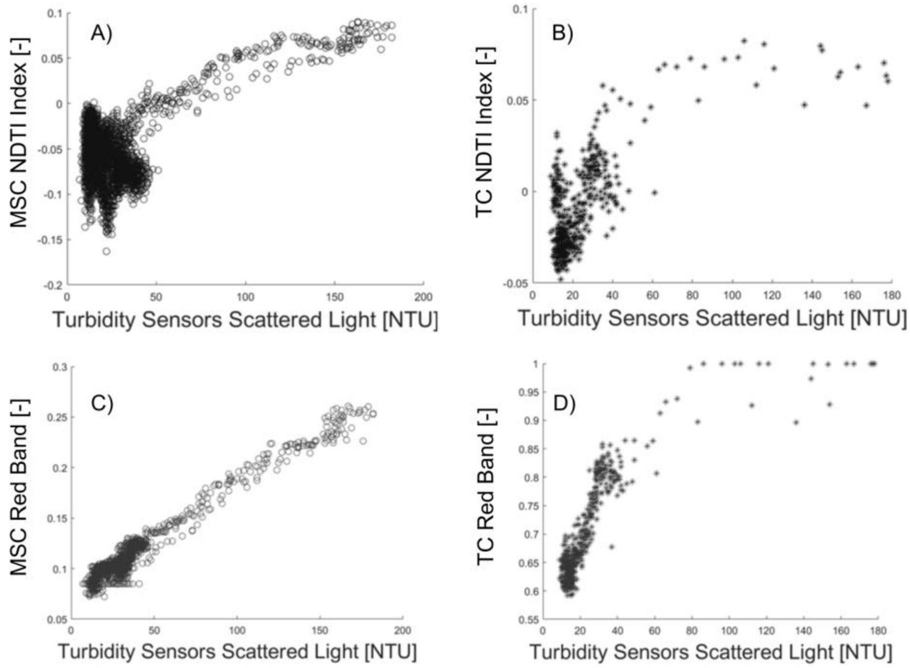

Figure 3.10: Scatter plots of turbidity measurements compared with MSC red band (C) and NDTI (A) and TC red band (D) and NDTI (B)

Figure 3.10 confirms the performance of MSC and TC indices and bands in relation to sensor's data. The MSC red band (C) shows a strong linear correlation with turbidity, while the NDTI index (A) exhibits a clear but less steep behaviour, after an initial dispersion of data for low turbidity level. In contrast, the TC red band (Figure 3.9D) provides a positive correlation, particularly at lower turbidity levels (below 80 NTU), while the scatter becomes more spread out at higher NTU values.

NDTI in TC (Figure 3.9B) reveals a more dispersed distribution, especially for high turbidity values, potentially due to a non-linear behaviour of the index under these conditions.

3.3.2 Combination of the experimental results

Looking at Figure 3.11, It is worth noting that there is a substantial gap in starting PI values recorded by the camera in both the field experiments, while their increments are comparable with all the recorded turbidity peaks.

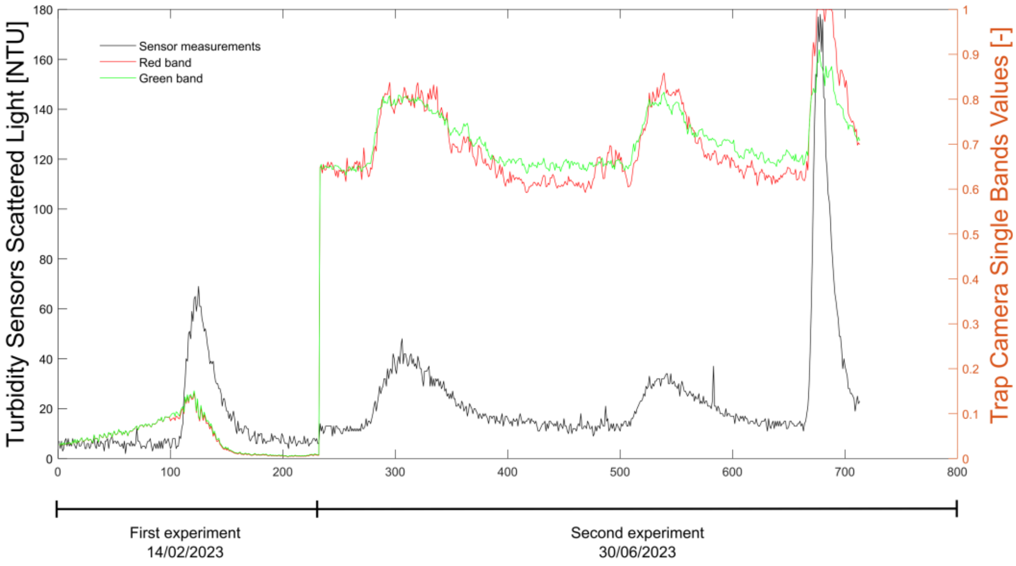

Figure 3.11: Comparison between turbidimeter measurements and trap camera red and green bands data for all the combined synthetic turbidity events of February and June 2023

This may be due to several factors, such as variation of light condition, sediment type and concentration, camera setup and sensitivity, water flow and composition.

Considering the similarities of the two designed experiments, the main cause was the difference in water levels within the monitored river section, between February and June 2023(see sections 2.3 and 3.1). The shallow water reached in the second experiment led to a considerable influence on the total water reflectance detected by the camera lens. Thus, the visibility of the riverbed could introduce background noise in the measurements, elevating the red and green band values independently of the actual concentration of suspended sediments in the water. This further highlights the need to consider background reflectance effects in shallow waters, especially during periods of low turbidity where the water column is relatively clear, as better described in sections 2.1 and showed in 3.2.

In addition, we can observe that the camera sensitivity also plays an important role in the comparability of the two experiments under different hydrological conditions, showing a significantly larger gap for starting PI values in TC data than for MSC data.

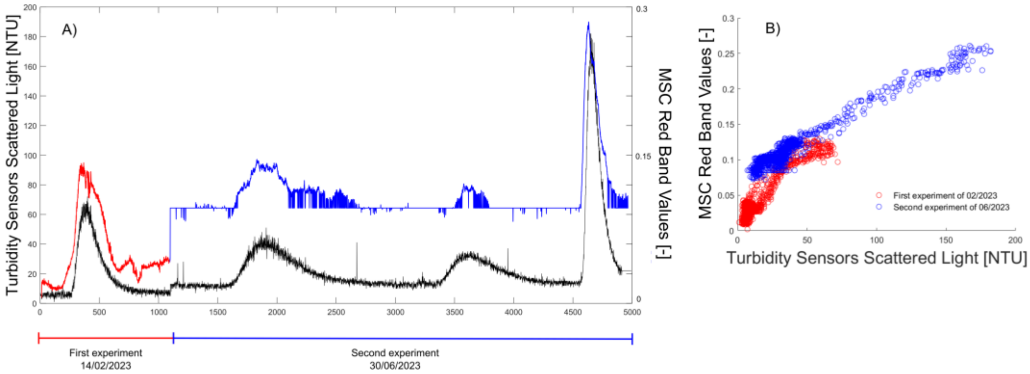

Figure 3.12: A) Comparison between turbidimeter measurements and MSC red band data for all the combined synthetic turbidity events of February (in red) and June (in blue) 2023; B) Scatter plot of the variables.

Figure 3.12 displays a more consistent relationship between MSC red band data and turbidity across both experiments, while Figure 3.11 reveals that the TC data are more affected by external conditions, leading to less direct comparability between the two experiments. This suggests that the MSC sensor provides more stable and reliable data for turbidity monitoring, especially when comparing results from different time periods.

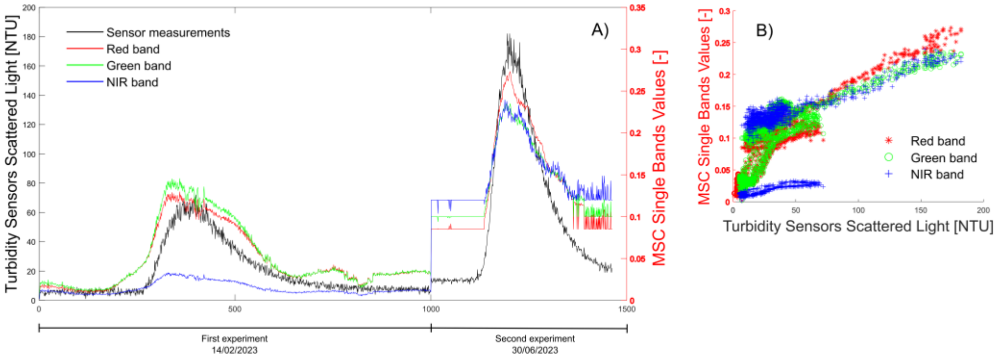

Figure 3.13: A) Comparison between turbidimeter measurements and MSC red, green and NIR bands data for the two main synthetic turbidity events of February and June 2023; B) Scatter plot of the variables.

Figure 3.13 takes into account only the two main peaks of the combined events. Two distinct trends emerge for low and high turbidity conditions, with differences in how the MSC single bands respond, especially for NIR band.

At low-moderate turbidity levels (NTU < 50), the red band shows a robust and linear relationship with turbidity, the green band displays more variability, probably due to the influence of the environmental noise, while the NIR band isn’t really reflected.

As turbidity increases beyond 50 NTU, all bands show more linear and less spread out results. The red band exhibits the strongest correlation with turbidity for both low and high turbidity conditions, during the two events.

Whit this in mind, in order to properly compare the results of the combined experiments, we assumed to consider the incremental variations of the band values R_{ROI}, starting from $R_{0\ ROI}$, that is a baseline value corresponding to the clear water condition of the specific monitored event, within the fixed ROI of the water surface.

Figure 3.14 displays the TC results as incremental variations $R_{ROI} - R_{0\ ROI}$ of red and green bands, compared to turbidity measures for all the events of the combined experiments. The close alignment of data points in the scatter plot in Figure 3.14B indicates a reliable match, suggesting that trap camera measurements can serve as a valuable tool for estimating turbidity levels, even with significant changes in hydrological and environmental conditions.

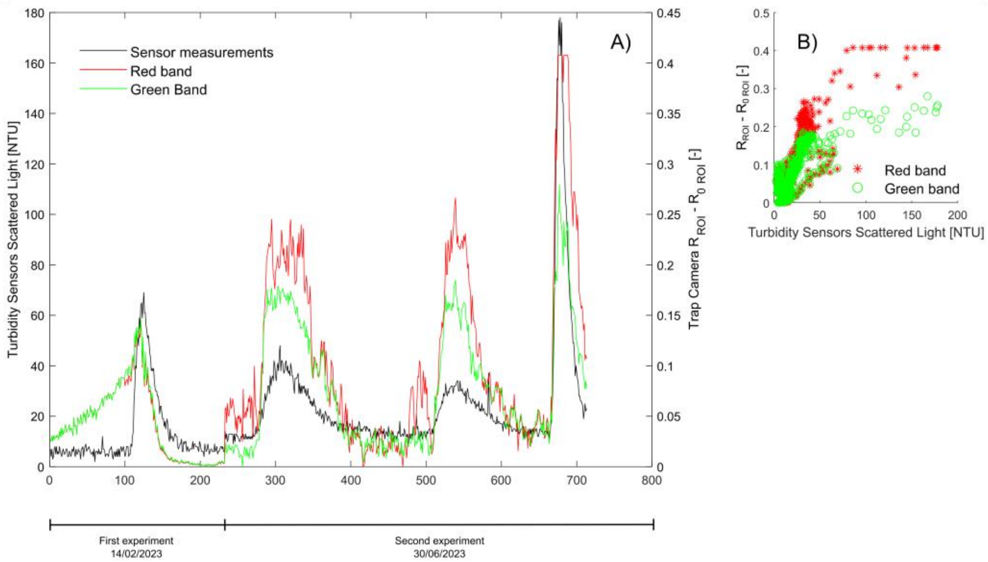

Figure 3.14: A) Comparison between turbidimeter measurements and trap camera red and green bands increments for all the combined synthetic turbidity events of February and June 2023, starting from bands values for a clear water condition ($R_{0\ ROI}$); B) Scatter plot of the variables.

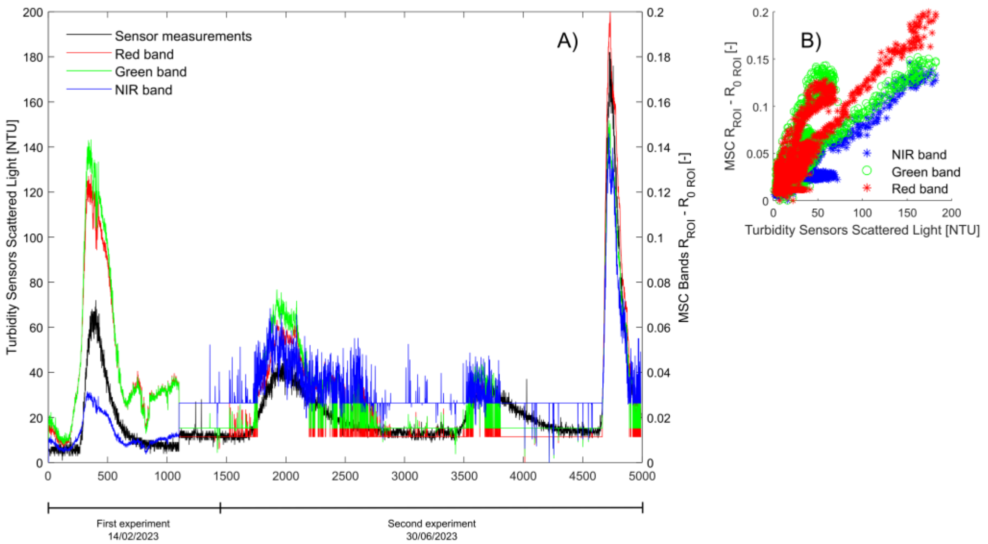

Figure 3.15: A) Comparison between turbidimeter measurements and MSC red, green and NIR bands increments for all the combined synthetic turbidity events of February

and June 2023, starting from bands values for a clear water condition ($R_{0\ ROI}$); B) Scatter plot of the variables.

The same approach was followed for MSC results in Figure 3.15.

In this case, all the bands show a strong linear correlation with the sensor readings, especially for high turbidity levels. In particular the red band seems to be, once again, the most sensitive wavelength to variations.

The presence of a wide scatter at lower turbidity levels (NTU < 50) highlights the challenges in interpreting also multispectral data under clearer conditions. In detail, we observe for the first event an underestimation of turbidity level from NIR band, while on the contrary there is a slight overestimation from red and green bands. Nevertheless, the improved correlation at higher turbidity underscores the effectiveness of MSC monitoring in such scenarios.

4 Discussion

In Section 4, all the results achieved during the experiments are discussed.
In particular, the performance metrics of both the two single experiments and their combination are evaluated. To follow, the range of applications and the reliability of the procedure have been analysed.

4.1 Performance metrics

4.1.1 First experiment performance

The first experiment of February 2023 was characterized by a great variety of camera types and installation setups, making it ideal for the analysis of the performance of all its variables. Table 2 summarizes the performance in terms of linear and quadratic R-squared correlation coefficients, considering the different camera types, bands, view angles, and installation setups selected for the field tests.

		BRIDGE				ZENITHAL VIEW		LEFT BANK		RIGHT BANK	
		M.S. CAMERA		TRAP CAMERA		DRONE		TRAP CAMERA		TRAP CAMERA	
		LIN.R^2	QUAD.R^2	LIN.R^2	QUAD.R^2	LIN.R^2	QUAD.R^2	LIN.R^2	QUAD.R^2	LIN.R^2	QUAD.R^2
SINGLE BANDS	RED BAND	0.89	0.91	0.25	0.31	0.76	0.88	0.82	0.85	0.89	0.89
	GREEN BAND	0.91	0.92	0.27	0.32	0.83	0.90	0.82	0.85	0.88	0.88
BAND RATIOS	RED/GREEN	0.12	0.16	0.01	0.06	0.01	0.34	0.59	0.64	0.37	0.38
INDEXES	NDTI	0.11	0.15	0.01	0.07	0.01	0.34	0.58	0.63	0.38	0.39
	NDWI	0.52	0.65								

Table 4.1: Linear and quadratic correlation coefficients R^2 of the camera bands compared to turbidity measurements, considering different camera types and installation points selected for the experiment of February 2023.

Red and green single bands can describe turbidity variations better than band ratios and indexes, for all the cameras used in this short-term experiment. Moreover, the MSC installation allowed us to understand the potential uses of bands beyond the visible spectrum. NIR band seems to have good performance for high concentration of suspended particles that reflect a consistent part of its radiation. In fact, considering combined MSC bands, the best performance comes from the NDWI index that involves the NIR and green bands.

For a proper comparison of all the variables, we decided to normalize then, as shown in Figure 4.1, since the data came from several sources, such as turbidity sensors and camera bands. The min-max normalization was chosen as the most suitable technique for our analysis because it scales the variables to a common range from 0 to 1, enabling direct comparison of their trends despite differences in units and ranges. This helps highlight correlations between the sensor readings and camera outputs during the turbidity event, preserving the shape of the original distribution and maintaining relative relationships between data points.

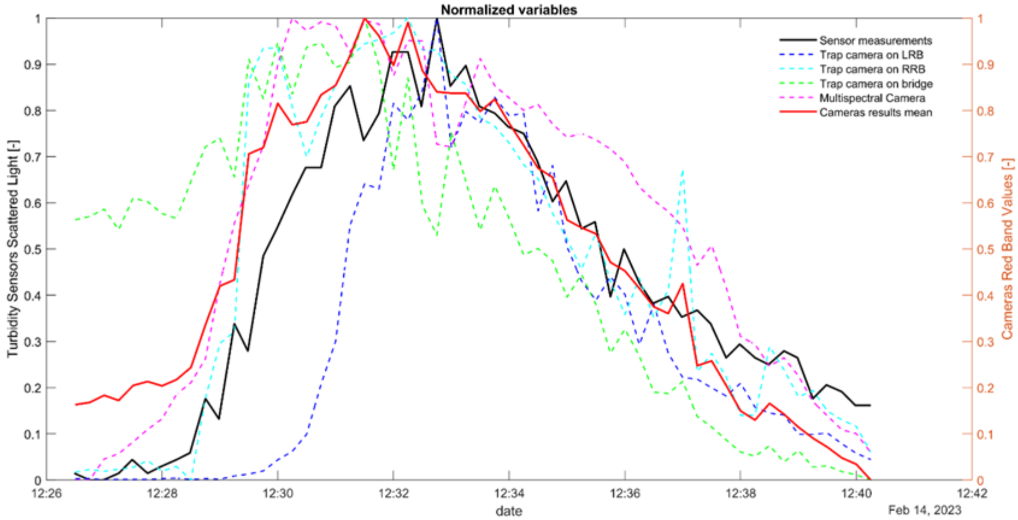

Figure 4.1: Comparison of normalized turbidimeter measurements and cameras red band values during the experiment

Within the Figure 4.1, the mean of all the normalized camera bands values is also reported in red. The normalization made it easier to assess camera performances in relation to the measurements of turbidity. Additionally, it enables a consistent comparison among different camera types, avoiding the issue of the Bayer pattern, used in digital cameras, that provides us RGB values already interpolated, unlike the multispectral camera that measures pure bands.

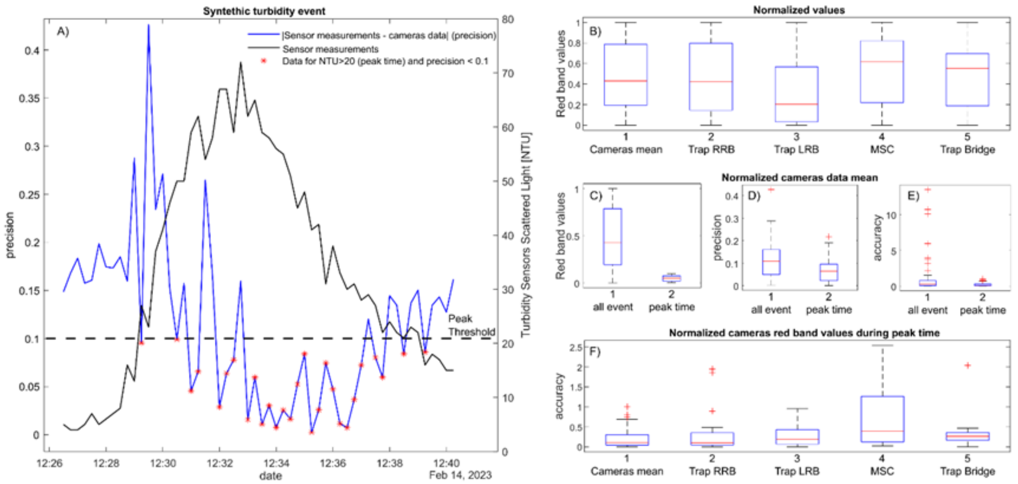

Figure 4.2: Plots of results precision (A, D) and accuracy (E, F) for each camera (B), considering the entire turbidity event and only the peak time (C, D, E, F).

Figure 4.2 describes the performance during a synthetic event of February 2023, focusing on precision and accuracy. The precision is meant as the absolute difference between the turbidimeter measures and the camera data, while the accuracy as this difference divided by the measures, which represents the percentage of the error. In particular, Figure 4.2A shows the precision of the mean of the normalized camera bands. The red dots in this picture show the lower discrepancy between the measures and the image data, pointing out higher reliability of the camera data in reflecting the turbidity levels, during the peak time, from 12:29 to 12:39, for the actual increase of turbidity (NTU>20).

Figure 4.2B describes the normalized red band values for five different cameras over the entire event. The results show that most cameras exhibit a relatively similar means and range of values, except for the LRB TC presenting lower values but still aligned with the measures.

Figures 4.2C, D and E highlight again the less range of variability and the best matching of the camera data with the sensor readings, during the peak time rather than the entire event.

Figure 4.2F illustrates the behaviour of normalized red band values of the different camera types during the turbidity peak time. It shows notable variability between the cameras. On one hand, MSC results display the largest spread, indicating lower accuracy than TCs. On the other hand, MSC box plot, together with LRB TC, is the only one without outliers and point standing on the whiskers, explaining his very good correlation with measurements reported in Table 4.1.

Overall, the results from both the short- and long-term data suggest us that the camera lens sensibility is not the only factor to consider. Camera orientation, installation setups, bands available, and also the intensity of the measured event can influence the monitoring performance.

4.1.2 Second experiment performance

		M.S. CAMERA		TRAP CAMERA		DIGITAL CAMERA	
		LIN.R^2	QUAD.R^2	LIN.R^2	QUAD.R^2	LIN.R^2	QUAD.R^2
SINGLE BANDS	RED BAND	0.90	0.91	0.67	0.87	0.60	0.61
	GREEN BAND	0.82	0.85	0.56	0.83	0.63	0.64
BAND RATIOS	RED/GREEN	0.70	0.71	0.52	0.60	0.16	0.17
INDEXES	NDTI	0.67	0.68	0.50	0.59	0.15	0.16
	NDWI	0.34	0.60				

Table 4.2: Linear and quadratic correlation coefficients R^2 of the camera bands compared to turbidity measurements, considering different camera types for the experiment of June 2023.

The performance metrics from Table 4.2 indicate that the M.S. Camera has the highest correlation with turbidity measurements, particularly in the Red Band, with R^2 values of 0.90 for linear and 0.91 for quadratic regressions. The Trap Camera also performs well in the Red Band, with R^2 values of 0.67 and 0.87 for linear and quadratic, respectively. However, it shows lower correlations in other bands. The Digital Camera exhibits the lowest correlation coefficients across all bands, with the highest being 0.63 for linear and 0.64 for quadratic in the green band. These metrics highlight the MS camera as the most reliable for environmental monitoring and water quality assessment. This information is crucial for selecting appropriate instruments for further investigations. In fact, the reliable performance metrics of trap camera, that was the most cost-effective camera, suggests its possible spreading for river basin monitoring applications.

4.1.3 Performance of the combined experiments

		ALL TURBIDITY EVENTS				TWO MAIN TURBIDITY EVENTS			
		M.S. CAMERA		TRAP CAMERA		M.S. CAMERA		TRAP CAMERA	
		LIN.R^2	QUAD.R^2	LIN.R^2	QUAD.R^2	LIN.R^2	QUAD.R^2	LIN.R^2	QUAD.R^2
SINGLE BANDS	RED BAND	0.68	0.71	0.19	0.28	0.89	0.92	0.50	0.52
	GREEN BAND	0.50	0.57	0.13	0.24	0.80	0.88	0.45	0.47
BAND RATIOS	RED/GREEN	0.20	0.30	0.34	0.36	0.26	0.34	0.40	0.41
INDEXES	NDTI	0.19	0.27	0.32	0.34	0.24	0.31	0.37	0.38
	NDWI	0.00	0.00			0.10	0.11		

Table 4.3: Linear and quadratic correlation coefficients R^2 of the MSC and TC bands compared to turbidity measurements, considering all the turbidity events in the combined experiments of February and June 2023.

The performance metrics of Table 4.3 shows the degree of correlation between camera data and turbidimeter measures for the combined experiments of February and June 2023. They indicate that the MS camera outperforms the trap camera across all bands, with especially high correlations in the red band during the most significant turbidity events. Despite this, the trap camera shows reasonable performance for the red and green bands during the two higher turbidity events.

		ALL TURBIDITY EVENTS			
		M.S. CAMERA		TRAP CAMERA	
		LIN.R^2	QUAD.R^2	LIN.R^2	QUAD.R^2
SINGLE BANDS	RED BAND	0.75	0.75	0.63	0.70
	GREEN BAND	0.62	0.67	0.54	0.65
	NIR BAND	0.72	0.73		

Table 4.4: Linear and quadratic correlation coefficients R^2 of the incremental variation R_{ROI} - $R_{0\ ROI}$ of MSC and TC bands compared to turbidity measurements, considering all the turbidity events in the combined experiments of February and June 2023.

Table 4.4 confirms the reliability of the procedure also for changing hydrological conditions, considering the incremental variation R_{ROI} - $R_{0\ ROI}$. Once again, the performance metrics show that the MS camera consistently outperforms the trap camera across all bands. In terms of increments, the MSC NIR band provides a strong match, also better than green band. This time, the trap camera also shows solid results, particularly for the red band values. Notably, the red band appears as a critical indicator for turbidity assessment, given its higher correlation in both cameras. This demonstrates the potential of the trap camera as a budget-friendly alternative for practical applications and support for water quality monitoring.

4.2 Range of applications

Regarding the first experimental setup, the presence of the submerged turbidimeters in both river sides (Figure 4) ensured to quantify the horizontal variability of the turbidity level along the river cross section. Its vertical variability on the water column is not so significant for a river as small as Selke, with a registered maximum water level of 1 meter. However, the proposed image-based procedure shall also apply for bigger rivers, since cameras capture the light from the entire water column until a mid-high turbidity level is reached. Once achieved this threshold (Figure 2.b), only the water surface can be investigated by the camera.

Interesting results were observed for all three RGB bands, since we used a white clay to increase the turbidity level. Further experiments with multiple tracers as inputs, changing the colours and particle concentrations will help to gauge the effectiveness of the procedure. What we expect from a generalized application of the procedure, on the light of this and the past field tests experiences (Miglino et al., 2022), is the greater reliability of the red band, for variable suspended particles characteristics, and better performances of band ratios and indexes, for long term monitoring in different hydrological conditions.

The comparison of all experimental data in Figure 4.3.a shows that the initial band signal responses were different for each camera, depending on lens sensitivity, position, field of view, angles from water surface and orientation with respect to the sun's apparent motion axis. One way to homogenize these results is to consider the increment of band signals, starting from a band signal for clear water condition, referred to the image frame with minimum measured NTU value. Figure 13.b shows the increments between the red band signals (Red) for each frame and for the clear water conditions (Red_0). Since the UAV data was split into two distinct videos, some of the primary turbidity event occurred during the pause between the two recordings, hence it was excluded. In addition, the UAV camera was the only one with a pre-set automatic light balance, making it impossible to integrate these data with the others.

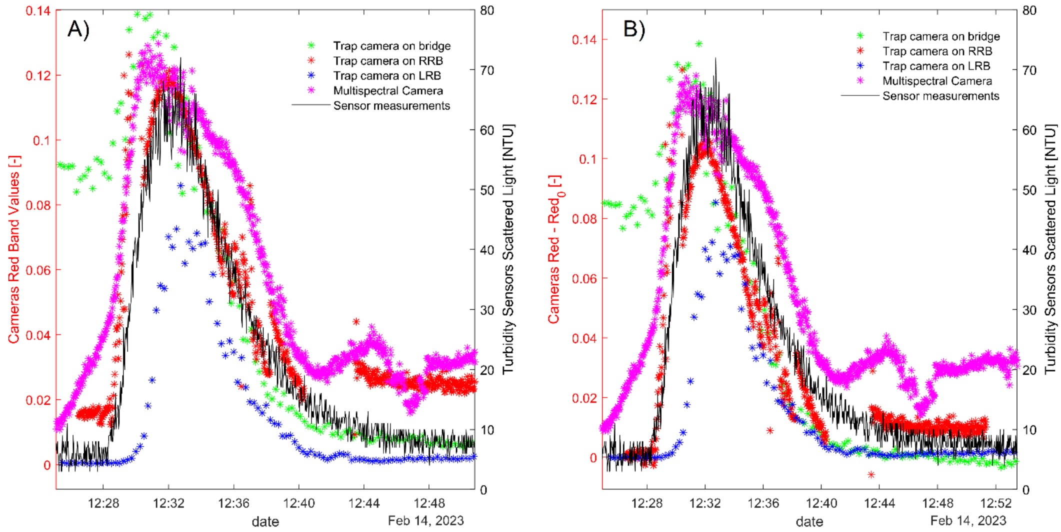

Figure 4.3: Comparison of turbidimeter measurements and all the cameras' data, in terms of red band values (A) and red band increments (B), starting from a clear water condition (Red_0), during the first experiment of February 2023.

It is worth to observe how there is a better overlap for the Red- Red_0 increment curves than the single red band signal curves. In fact, the identification of the PI for the clear water could remove the mismatches between the initial PIs detected by the camera, both due to changes in light and camera lens sensitivity. Next experiments will face this issue, especially for shallow water conditions, where the visibility of the riverbed background could become a reference value of water clarity, regardless of site- and time- specific variabilities.

The second experiment confirmed the reliability of the procedure also for tracers changing in colour, granulometry and concentration. Figure 4.4 shows that all the three peaks generated by kaolin, dolomite and lava flours were well detected by the camera monitoring, presenting a lower correlation for the second turbidity event, probably due to a lower concentration of dolomite particles than the other two tracers. Indeed, these results confirmed that the camera monitoring procedure is not affected by the characteristics of the tracer, but that it's less reliable for low turbidity events (NTU<30).

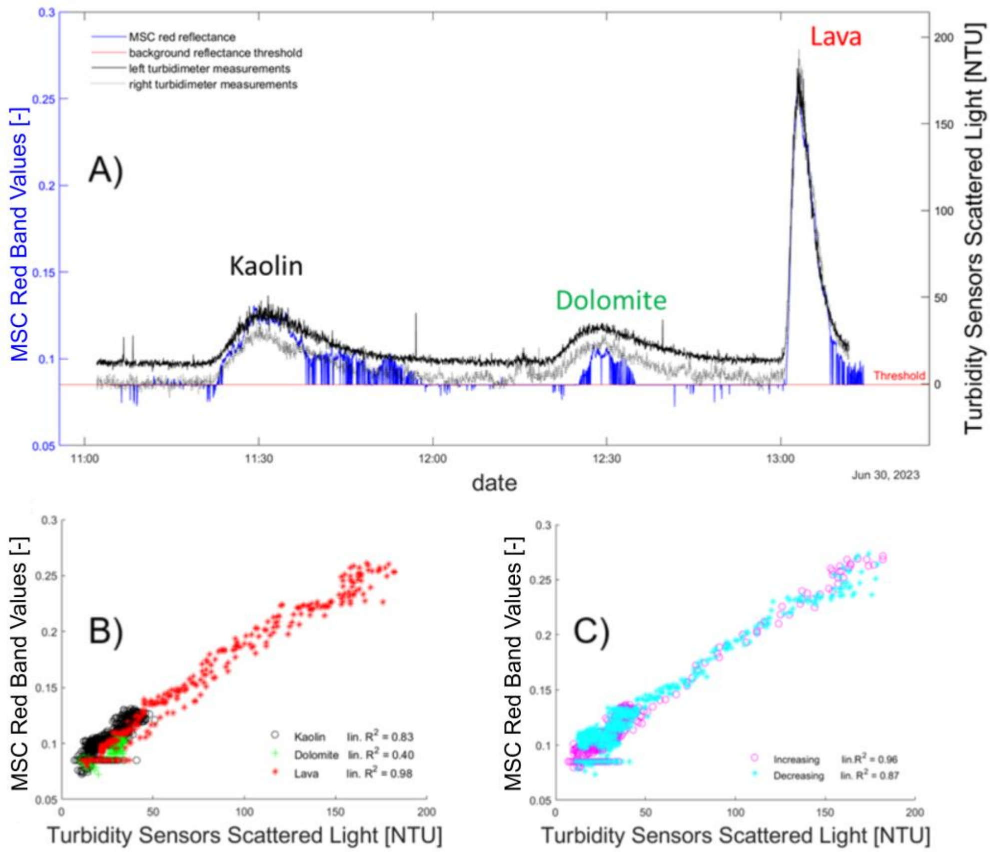

Figure 4.4: A) Comparison of turbidimeter measurements and the MSC red band data, considering the three consecutive turbidity events generated by different tracers (kaolin, dolomite and lava flours); B) Scatter plots of the three turbidity events, taken individually; C) Scatter plots of the turbidity events, separated by turbidity level increasing and decreasing curves

Moreover, Figure 4.4 highlights also good correlations both for the increasing and decreasing phases of the turbidity level, that means that the camera systems are able to estimate the start and the end of an event within a real riverine environment.

4.3 Spatial variability and active pixel count within the region of interest

In our investigations, only the mean of the active pixels within the RoI is considered as a proxy for turbidity. For active pixels, we mean the processed pixels with information on the actual water reflectance. The image processing procedure allowed us to minimize the misinformation from the images, reducing the effect of changing light conditions with radiometric calibration, and removing saturated pixels or in strongly shaded areas with binarization. Nevertheless, the spatial variability of the pixel intensities and the availability of active pixels within a RoI of a single image could be critical factors that need to be analyzed.

The following Figures 4.5, 5R, 6R, and 7R describe the variability of the standard deviation and the active pixels count, for both MSC and TC camera, during the field experiment of February 2023.

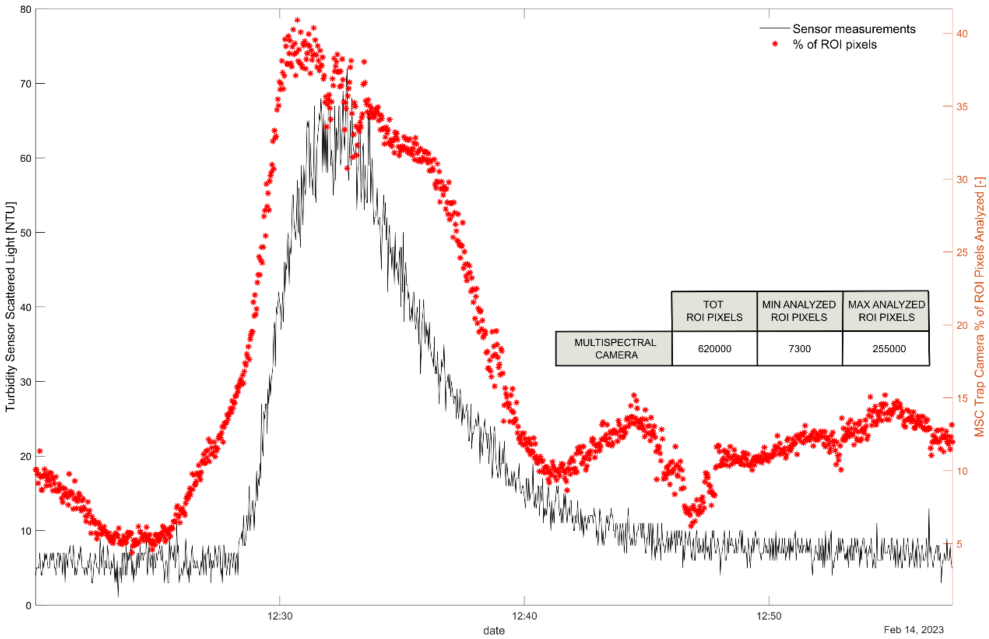

Figure 4.5: Comparison of turbidimeter measurements (in black) and number of analyzed ROI pixels in MSC data (in red) during the short-term experiment of February 2023

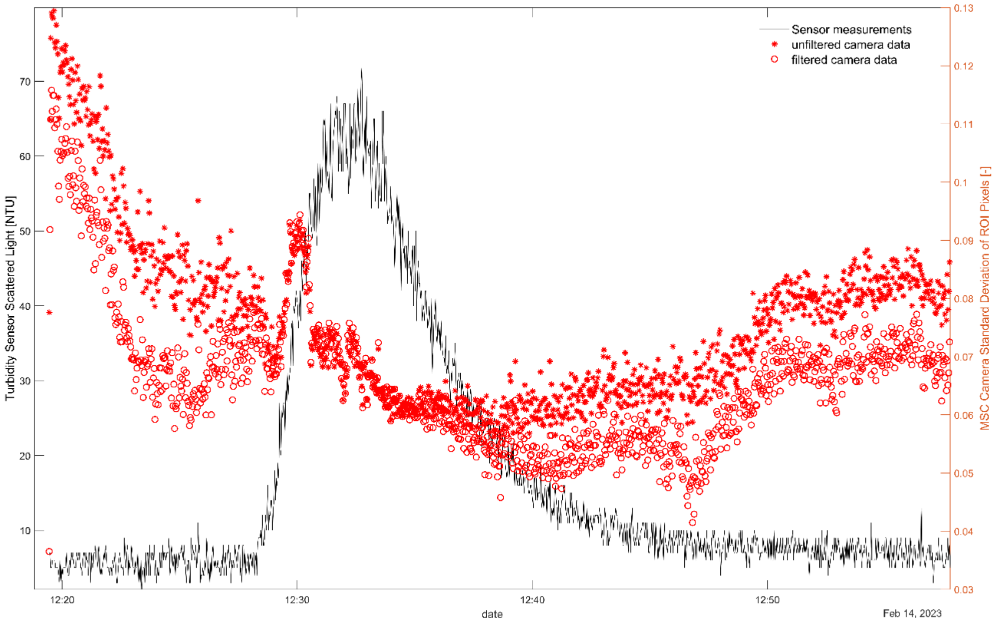

Figure 4.6: Comparison of turbidimeter measurements (in black) and the standard deviation of ROI pixels intensity in multispectral camera red band (in red), during the short-term experiment of February 2023

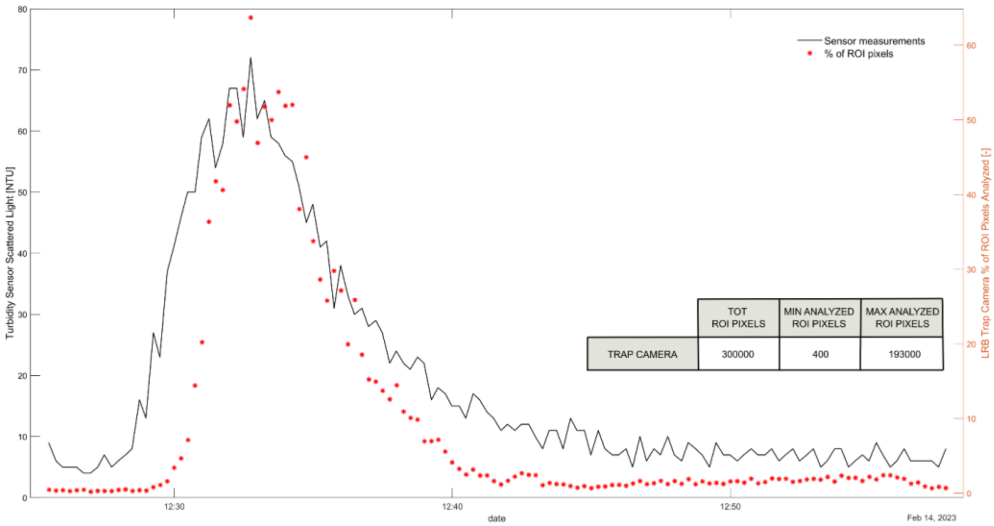

Figure 4.7: Comparison of turbidimeter measurements (in black) and number of analyzed ROI pixels in LRB trap camera data (in red) during the short-term experiment of February 2023

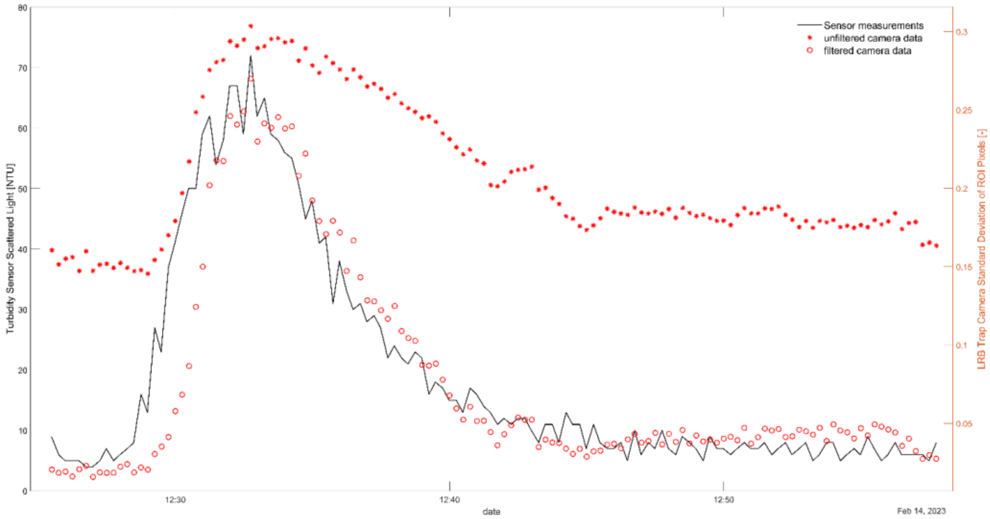

Figure 4.8: Comparison of turbidimeter measurements (in black) and the standard deviation of ROI pixels intensity in LRB trap camera red band (in red), during the short-term experiment of February 2023

It is worth to observe that the active pixel count is directly proportional to the turbidity level, both for MSC (Figure 4.5) and trap camera (Figure 4.7). These results show that the resolution of the camera and its distance from the water must be considered to ensure a minimum number of active pixels for less sensitive camera, such as the trap camera, especially when the water is clear.

In Figures 4.6 and 4.8, it is evident that the image filtering procedure of both the camera data, significantly reduces the standard devations of the RoI pixels intensity, in particular for low-moderate turbidity conditions, where its spatial variability is particulary high for the unfiltered data.

Finally, these figures confirm the effectiveness of the procedure in enhancing the overall river turbidty level using cameras, even if the shown PI standard deviation values are still non negligible.

5 Conclusions

In the first part of Section 5, a brief summary of the study is shown.
To follow, the importance of developing this procedure and of its implications in real river monitoring practises has been deepened.
Lastly, the future research directions have been outlined.

5.1 Summary of the study and key findings

The proposed research work investigated the potential of camera image analysis in estimating the river quality status, in particular focusing on water turbidity, since it is a critical parameter directly and indirectly related to many suspended pollutants.
A survey within the Bode River basin was done to find the best location where to perform the planned field experiments. Meisdorf monitoring station was chosen as the most suitable river section for our campaigns. The field activities involved a first phase of continuous long-term monitoring (Section 1.5.1), by fixing a trap camera beside the river and following the seasonal variability of turbidity level, mainly related to flood events. Afterwards, two field experiments in February and June 2023 (Section 2 and Section 3) aimed to understand the capability of several camera types and installation setups to monitor the river turbidity events, artificially recreated using clay tracers with different colours and concentrations, under varying light and flow conditions.
The experimental activities revealed that single RGB and NIR bands values were the most reliable proxy for turbidity monitoring in short-term observations, better than band ratios and indexes. The opposite could be true for long term observations, since single band signal tends to be more influenced by the variability of light and flow conditions. Field tests proved that cameras, even the cheap models, can produce reliable estimates continuously in time. With the ability to collect near real-time turbidity data, the methodology supports timely interventions in water resource management. Prompt action during pollution events enables public health protection and proactive ecosystem management. The thesis bridges civil systems engineering, environmental science, and technology, promoting collaborative research. It opens

avenues for partnerships among engineers, ecologists, hydrologists, and data scientists to address complex river management issues.

5.2 Implications in river monitoring practices

Prior to this work, image analysis for water turbidity was predominantly conducted using satellite data for large rivers or camera data and specific optical sensors in laboratory. The added value of our study lies in the development of a monitoring procedure that can be directly implemented on-site, without spatial and temporal limitations of data acquisition. This allowed us to test the method under real conditions and to optimize the camera installation for future applications in various environments.

By combining image analysis techniques with field data collection, the thesis wants to demonstrate how digital technologies can be integrated into environmental monitoring practices. This fusion of civil engineering principles with computer vision technologies highlights the thesis's relevance to both engineering and environmental science disciplines.

The proposed image processing procedure offers significant advances in river monitoring practices by providing a near real-time, continuous, and automated system for water turbidity assessment. By facilitating frequent and automated monitoring, the research contributes to the ability to track fast changes in turbidity in response to environmental events, such as flash floods or pollution incidents.

Moreover, they can be easily and frequently installed without excessive costs, along the whole river network, providing a comprehensive knowledge of the river basin status. Indeed, this approach can complement current monitoring practices, addressing their limitations in data availability and resolution, especially for small or inaccessible rivers where existing methods are impracticable. Furthermore, the use of these sensors minimizes environmental disturbance, aligning with sustainable monitoring practices. The widespread of this procedure could significantly increase the amount of available information on water status at basin scale. By enhancing the reliability of turbidity's relationship with environmental factors and its role in the transport of pollutants, the thesis contributes to deeply understand the ecohydrological dynamics involved in river processes.

5.3 Future research directions

On-site tests are still on-going in two different case studies. In particular, in Bode River a trap camera is providing continuous long-term monitoring of actual turbidity events. This will allow us to acquire a significant set of data, covering many environmental and hydrological conditions, to fully understand how to optimize the characteristics of the camera and the installation setups for real monitoring applications.

Moreover, another camera is installed in the Sarno River section, within the RiverWatch project activities and in collaboration with "Consorzio di Bonifica Integrale Comprensorio Sarno". It is a relevant case study to outline innovative and effective guidelines for water quality monitoring and water pollution prevention, since it is one of the most polluted rivers in Europe and it directly involved us. For these reasons, the current research activities are aimed at creating an innovative early warning network, not only limited to turbidity, but also provide a great potential for other water quality (e.g. chlorophyll-a) and water related (e.g. macroplastic) monitoring applications, advancing and supporting the existing river monitoring techniques.

The next natural step is the involvement of these water quality prediction algorithms in a citizen science approach. Within this context, our research group is developing a smartphone app for river monitoring (https://sites.google.com/view/riverwatch/home-page?authuser=0), focusing in particular on macroplastics and turbidity, that are the most easy-to-capture water quality information collectable by the people. The real implementation of a continuous image-based river monitoring network like this, can offer new options to water resources management strategies and the preservation of aquatic ecosystems.

Data Availability

The experiment data can be provided by the corresponding author upon request.

Publications on the research activities

Miglino, D., Jomaa, S., Rode, M., Isgro, F. and Manfreda, S., Monitoring Water Turbidity Using Remote Sensing Techniques. Environmental Sciences Proceedings, 21(1), p.63, 2022.

Manfreda, S., Miglino, D., Saddi, K. C., Jomaa, S., Eltner, A., Perks, M., ... & Rode, M., Advancing River Monitoring Using Image-Based Techniques: Challenges and Opportunities. Hydrological Sciences Journal, 69(6), 657-677, 2024.

Saddi, K. C., Miglino, D., Isgro, F., van Emmerik, T. H., & Manfreda, S. Balancing Accuracy and Efficiency for River Plastic Monitoring. In IGARSS 2024-2024 IEEE International Geoscience and Remote Sensing Symposium (pp. 3836-3840). IEEE, 2024.

Miglino, D., Saddi, K., C., Isgrò, F., Jomaa, S., Rode, M. & Manfreda, S., Image Processing for Continuous River Turbidity Monitoring - Full Scale Tests and Potential Applications, https://doi.org/10.5194/egusphere-2024-2172 (under review).